nature biomedical engineering

SUPPLEMENTARY INFORMATION

https://doi.org/10.1038/s41551-018-0317-8

In the format provided by the authors and unedited.

DNA origami nanostructures can exhibit preferential renal uptake and alleviate acute kidney injury

Dawei Jiang[1,2,10], Zhilei Ge[3,4,10], Hyung-Jun Im[1,5,10], Christopher G. England[6], Dalong Ni[1], Junjun Hou[7], Luhao Zhang[7,8], Christopher J. Kutyreff[6], Yongjun Yan[1,6], Yan Liu[3], Steve Y. Cho[1,9], Jonathan W. Engle[6], Jiye Shi[7], Peng Huang[2*], Chunhai Fan[4,7*], Hao Yan[3*] and Weibo Cai[1,6,9*]

[1]Department of Radiology, University of Wisconsin–Madison, Madison, WI, USA. [2]Guangdong Key Laboratory for Biomedical Measurements and Ultrasound Imaging, Laboratory of Evolutionary Theranostics, School of Biomedical Engineering, Health Science Center, Shenzhen University, Shenzhen, China. [3]Biodesign Center for Molecular Design and Biomimetics, The Biodesign Institute, School of Molecular Sciences, Arizona State University, Tempe, AZ, USA. [4]School of Chemistry and Chemical Engineering, Institute of Molecular Medicine, Renji Hospital, School of Medicine, Shanghai Jiao Tong University, Shanghai, China. [5]Graduate School of Convergence Science and Technology, Seoul National University, Seoul, Republic of Korea. [6]Department of Medical Physics, University of Wisconsin–Madison, Madison, WI, USA. [7]Division of Physical Biology and Bioimaging Center, Shanghai Synchrotron Radiation Facility, CAS Key Laboratory of Interfacial Physics and Technology, Shanghai Institute of Applied Physics, Chinese Academy of Sciences, Shanghai, China. [8]Shanghai Key Laboratory of Green Chemistry and Chemical Processes, School of Chemistry and Molecular Engineering, East China Normal University, Shanghai, China. [9]University of Wisconsin Carbone Cancer Center, Madison, WI, USA. [10]These authors contributed equally: Dawei Jiang, Zhilei Ge, Hyung-Jun Im. *e-mail: peng.huang@szu.edu.cn; fanchunhai@sjtu.edu.cn; hao.yan@asu.edu; wcai@uwhealth.org

Supplementary Information

Table of Contents:

Methods

Materials

All staple DNA strands (lengths ranging from 20-60 bases) were purchased from Integrated DNA Technologies Inc. (www.IDTDNA.com) in the format of 96-well plates at 100-nmol synthesis scales with concentration normalized to 100 μM. These strands were directly used for self-assembly without any purification. M13mp18 single-stranded DNA scaffold (M13 ssDNA) were purchased from New England Biolabs (catalog number: N4040S) and used without further purification. All other chemicals or materials were purchased from Sigma-Aldrich and used as received unless stated otherwise.

Self-assembly of DNA origami nanostructures (DONs)

DONs with different shapes (rectangular, triangular, and tubular) were assembled by annealing a 7249-nt viral genome M13mp18 (M13 ssDNA, the template strand) with various sets of synthetic oligonucleotides (i.e. staple strands) of 20-60 bases. All DONs were prepared in 1 x TAE-Mg^{2+} (12.5 mM magnesium acetate, 2 mM EDTA, 20 mM acetic acid, and 40 mM Tris base, pH 8.0) with an established method[1]. For each DON, 20 nM circular M13 ssDNA was mixed with a set of 10-fold molar excess of staple strands. The mixture was annealed from 90 ºC to 4 ºC with a temperature gradient shown in **Table S1**. The annealed solution was filtered with 100 kDa Amicon ultrafilters in 1 x TAE-Mg^{2+} buffer or phosphate-buffered saline-magnesium (PBS-Mg^{2+}, 12.5 mM magnesium acetate, pH 7.2-7.5). The purity of DONs was examined via

agarose gel electrophoresis (AGE). The concentration of DONs was measured by their absorbance at 260 nm, with an average extinction coefficient of 109,119,009 $M^{-1}cm^{-1}$. DNA tetrahedron nanoparticle (DTN) with four overhangs was assembled following previous reports[2, 3]. In brief, four pre-designed oligonucleotides (1 μM) were mixed in 1 x TAE-Mg^{2+} buffer and annealed from 95 ºC to 4 ºC (**Supplementary Table S4**). Partially-folded DONs were assembled with incomplete sets of staple strands and used as controls in this study. For detailed design and sequences of DONs, please see **Supplementary Figure S1 – S18, and Supplementary Sheet 1-3**.

Atomic Force Microscopy (AFM) imaging of DONs

DONs (2 μL, 20 nM) was deposited onto a freshly cleaved mica cell and left to adsorb for 2-3 min. 1 x TAE-Mg^{2+} buffer (400 μL) was added to the liquid cell, and the sample was scanned in a tapping mode under fluid on a Pico-Plus AFM (Agilent Technologies, Santa Clara, CA, USA) with NP-S tips (Veeco, Inc., Oyster Bay, NY, USA).

Transmission Electron Microscopy (TEM) imaging of DONs

TEM grids (400 mesh, copper grid coated with ultrathin carbon, Ted Pella) were glow discharged (Emitech K100X). 2 μL concentrated samples were deposited onto the grids for 1 min, washed with 10 μL DI water for 5 sec, stained with 10 μL of 1% uranyl formate twice (2 sec for the first time and 15 sec for the second time), and imaged using Philips CM12 transmission electron microscope. The grid was touched with a drop of 0.7 % uranyl formate solution and excess solution was wicked away with a

filter paper. Again the grid was touched with the second drop of uranyl formate solution for 15 seconds, and the excess solution was removed with a filter paper. To evaporate extra solution, the grid was kept at room temperature. Low-resolution TEM studies were conducted by using a Philips CM12 transmission electron microscope, operated at 80 kV in the bright field mode.

Agarose Gel Electrophoresis

0.8% Agarose Gel Electrophoresis (AGE) was performed in 1 x TAE/Mg buffer (Tris-acetic acid 40 mM, pH 8.0, magnesium acetate 12.5 mM, EDTA 1 mM) at 80 V and 4 ^{o}C for 1.5 h. Then DONs were stained with ethidium bromide for 5 min for further analysis on a chemiluminescence imaging system.

Dynamic Light Scattering Measurements

Measurements were made on a Zetasizer, Nano Series, Nano ZS machine made by Malvern Instruments. Dispersion technology software with a standard setting was used for data analysis (also from Malvern Instruments).

Zeta-potential Measurements

The zeta potential of DONs was determined with a Malvern ZetaSizer Nano (Malvern Instruments) by taking the average of four samples at a final concentration of 20 nM in 1×TAE/Mg^{2+} buffer at pH 8.0 using a disposable zeta cell. Data were then analyzed using the Malvern Instrument Dispersion Technology Software.

^{64}Cu-labeling of DONs

Radiolabeling of DONs was achieved by hybridizing ^{64}Cu-labeled single-stranded DNA (ssDNA) with side-arms designed on DONs. Amine group-functionalized ssDNA was mixed with 2-S-(4-Isothiocyanatobenzyl)

-1,4,7-triazacyclononane-1,4,7-triaceticacid (p-SCN-Bn-NOTA) in dimethyl sulfoxide (DMSO) and incubated at pH 8.5–9.0 at room temperature for 2 h. NOTA-ssDNA was purified using a PD-10 desalting column with 1 x PBS as the elution buffer. ^{64}Cu (decay half-life: 12.7 h) was produced by a PETtrace cyclotron (GE Healthcare) using the ^{64}Ni(p, n)^{64}Cu reaction. For the radiolabeling of NOTA-ssDNA, $^{64}CuCl_2$ was diluted with sodium acetate (0.1 M, pH 5.5) and mixed with NOTA-ssDNA. Following 1 h incubation at 37 ºC with constant shaking, the mixed solution was purified with a PD-10 column, and a fraction with the highest radioactivity was chosen to hybridize with DONs.

PET imaging and biodistribution study of DONs in healthy mice

10-50 μCi (0.37-1.85 MBq) of ^{64}Cu-labeled DONs, including M13 ssDNA, fully-folded DONs, or partially-folded DONs, were intravenously injected into healthy ICR mice. Longitudinal PET scans were performed with an Inveon microPET/microCT rodent model scanner (Siemens Medical Solutions, Erlangen, Germany) at 3, 12, and 24 h after injection. For Rec-DON, a CT model from Inveon database was aligned with PET imaging at 3 and 12 h after injection. Region-of-interest (ROI) analysis of all PET

images was performed to determine time-activity curves for different organs. To obtain ROI data, the manual delineations of major organs in animals were made on decay-corrected whole-body PET images using the in-house image analysis software (Inveon^{TM} Research Workplace, IRW). The counts/pixel obtained from the raw PET data was converted to counts/cm^3 based on a calibration coefficient obtained from phantom PET scans. By assuming the tissue density was approximately 1 g/cm^3, counts/cm^3 was converted to counts/gram, which was then divided by the injected dose to provide the final ROI in %ID/g. By doing this, we were able to calculate and subtract any leftover dose in the tail or possible contamination on the skin to better quantify the actual dose in organs/tissues of interest. After the scans at 24 h post-injection, mice were euthanized, and organs-of-interest were harvested to quantify the uptake of each DON using a gamma counter (PerkinElmer, Waltham, MA, USA). The tracer accumulation in each organ or tissue was presented as percentage of injected dose per gram of tissue (%ID/g, ≥ 3 mice in each group).

PET imaging and biodistribution study of ^{64}Cu-labeled single-stranded DNA (ssDNA) in healthy mice

Approximately 50 μCi (1.85 MBq) of ^{64}Cu-labeled ssDNA was intravenously injected into healthy ICR mice and serial PET scans were performed at 3, 12, and 24 h after injection. ROI analysis was used to analyze the tracer uptake in major organs. At 24 h post-injection, mice were euthanized and organs-of-interest were harvested to quantify the accumulation of each DNA nanostructure using a gamma counter

(PerkinElmer, Waltham, MA, USA). The tracer accumulation in each organ or tissue was presented as %ID/g (n=3).

Confocal imaging of fluorescently-labeled rectangular DNA origami nanostructure (Rec-DON) in kidneys

Cy3-labeled Rec-DON was *i.v.* injected into mice and kidneys were harvested at 10 min, 3 h, and 12 h after injection and stored in optimum cutting temperature (O.C.T.) specimen matrix (VWR, Radnor, PA, USA) for cryostat sectioning at -20 ºC. Sectioning was performed by the Experimental Pathology Laboratory at University of Wisconsin – Madison. Frozen kidney tissue slices of 5-µm thickness were washed with cold 1 x PBS. Then a cover glass was applied to each slide using Vectashield mounting medium (Vector Laboratories, Burlingame, CA, USA), and confocal imaging was performed using a Nikon A1R confocal microscope (Nikon Instruments, Melville, NY, USA).

PET imaging of Rec-DON in AKI mice

50 µCi (1.85 MBq) of ^{64}Cu-labeled Rec-DON was intravenously injected into murine models of AKI (n=3)and serial PET scans were performed at 5 min, 30 min, 1 h, 3 h, 6 h, 12 h, and 24 h after injection. ROI analysis was used to analyze the tracer uptake in major organs. At the 24 h time point, mice were euthanized, and organs-of-interest were harvested to quantify the accumulation of Rec-DON using a gamma counter

(PerkinElmer, Waltham, MA, USA). The tracer accumulation in each organ or tissue was presented as %ID/g (n=3).

Scavenging ABTS radicals with DONs

The free radical scavenging capability of DONs was tested based on the reduction of •$ABTS^+$ radicals by using the ABTS radical cation decolorization assay. 7 mmol of ABTS was dissolved in deionized water and reacted with 2.45 mM potassium persulfate to produce ABTS radical cation (•$ABTS^+$), and the mixture was kept in the dark at room temperature for 24 h before use. Then, the UV-Vis spectra of the pure solution of •$ABTS^+$ radicals and •$ABTS^+$ radical solution with M13 ssDNA or different DONs were monitored to measure the absorbance at 734 nm. The inhibition rate of •$ABTS^+$ radicals was calculated based on the ratio of neutralized •$ABTS^+$ radicals to overall radicals. All measurements were carried out in triplicate.

Scavenging hydroxyl and superoxide radicals with DONs

The hydroxyl radical scavenging efficiency was tested using a hydroxyl radical antioxidant capacity (HORAC) assay kit (Catalog number: STA-346-T. Cell Biolabs, Inc., USA). The superoxide radical scavenging efficiency was assessed with a SOD assay kit (Catalog number: CS1000. Sigma-Aldrich, USA). All tests were performed following the protocol provided by the kits.

Protection of cells exposed to H_2O_2 with DONs

Human embryonic kidney 293 (HEK293) cells were cultured at 37 °C with 5% CO_2 in Dulbecco's Modified Eagle Medium (DMEM) supplemented with 10% fetalbovine serum (FBS) and 1% penicillin/streptomycin. Cells were seeded into a 96-well cell culture plate at 10^6 cells/well and then incubated for 24 h at 37 °C under 5% CO_2. An equal mass of DONs, including M13 ssDNA, Rec-DON, Tri-DON, or Tub-DON, were added to cells and incubated for 30 min. The cells were then incubated with H_2O_2 (final concentration in each well: 250 μM) for 24 h at 37 °C with 5% CO_2. Colorimetric MTT assay was performed to examine the cell viability. To reliably measure reactive oxygen species (ROS) levels in live cells, a final concentration of 5 μM of fluorogenic probe (CellROX™ Deep Red Reagent) was added to the cells and incubated for 30 minutes at 37 °C after DONs incubation and H_2O_2 treatment. Afterwards, the cells were washed with 1 x PBS for three times and the emission at 665 was measured with an excitation of 640 nm.

FRET assay for examining the stability of DONs

Cy3/Cy5 dual-labeled Rec-DON was incubated in 80% serum or 50% urine and the FRET spectra were taken at 10 min, 3 h, and 12 h after incubation. Since the adjacent Cy3/Cy5 fluorophores were placed under the estimated Forster distance of ~5.6 nm, there will be Cy5 emission signal in Rec-DON when Cy3 excitation/Cy5 emission filters were used. If DONs were disassembled under the influence of enzyme in the FBS or the basic milieu of urine, the absence of FRET would cause a decrease in Cy5

signal intensity. FRET efficiency was calculated based on the Cy5 signal after Cy3 excitation (FRET efficiency was considered 100% at time 0).

Acute kidney injury (AKI) model establishment

All animal studies were conducted under a protocol approved by the University of Wisconsin Institutional Animal Care and Use Committee. Before initiation of the AKI model, all mice were deprived of water but had access to food for 15 h. At the end of the water restriction, 8 mL/kg of 50% glycerol was administrated into each hind limb of mice intramuscularly. All mice were then given free access to water and food[4, 5].

Treatment of AKI

Six groups of mice were studied: group 1 was healthy control mice (Healthy; n≥5) without any treatment, group 2 was AKI mice treated with 1 x PBS (PBS; n≥5), group 3 was AKI mice treated with 10 μg of M13 in 100 μL of 1 x PBS (, M13; n≥5), group 4 was AKI mice treated with 10 μg of Rec-DON in 100 μL of 1 x PBS (Rec-DON; n≥5), group 5 was AKI mice treated with 4.2 mg of NAC in 100 μL of 1 x PBS (H-NAC; n≥5), group 6 was AKI mice treated with 10 μg of NAC in 100 μL of 1 x PBS (L-NAC; n≥5). Two hours after the model induction, the agents were intravenously injected into AKI mice, and their kidney function was compared with that of healthy control mice. Please refer to **Supplementary Table S2 - S3** for more dose information about test materials for AKI treatment. To better illustrate the treatment of AKI using Rec-DON,

we further performed treatment using different doses of ssDNA, Rec-DON, and NAC. Please check **Supplementary Figure S45** for more details.

Dynamic ^{68}Ga-EDTA PET imaging for kidney function evaluation

^{68}Ga ($t_{1/2}$ = 68 min) was eluted from a ^{68}Ge/^{68}Ga radionuclide generator system (IDB Holland BV) with HCl (0.05 M) as the eluent. To prepare ^{68}Ga-EDTA, $^{68}GaCl_3$ was mixed with an equal volume of 10 mM EDTA in 2 x PBS buffer, and the final pH was adjusted to ~7.5 with $NaHCO_3$(1M)[6]. Radiochemical purity was determined using thin-layer chromatography silica gel plates developed with a solvent system of ammonium acetate buffer (1 M): methanol (v/v = 50:50).

For dynamic PET imaging using ^{68}Ga-EDTA, mice in the healthy control group or AKI treatment groups (n ≥ 3 for each group) were anesthetized with 2% isoflurane and their tail vein catheterized. Animals were placed on the PET bed in a prone position and sent into the scanner. Along with the *i.v.* injection of ^{68}Ga-EDTA (200-500 μCi), a 30-min dynamic PET scan was acquired simultaneously. The histogram files were divided into 28 frames: 6×10 s, 6×30 s, 6×60 s, and 10×120 s. Dynamic scans were reconstructed using an ordered subset expectation maximization 3D/maximum a posteriori (OSEM3D/MAP) reconstruction algorithm. ROI analysis of PET images was performed to determine the time-activity curve of the blood pool, kidneys, and bladder. Tracer uptake was expressed as %ID/g for the blood pool, and %ID for the kidneys and bladder.

Blood tests

24 hours after AKI initiation, mice in all groups were euthanized and blood samples were collected into pediatric heparin tubes (BD Biosciences, San Jose, CA, USA) and centrifuged at 2,000 x g for 15 min at 4 ºC, then the plasma was sent to the Clinical Pathology Laboratory in Veterinary Medical Teaching Hospital at University of Wisconsin – Madison for analysis of blood creatinine (Cr) levels and blood urea nitrogen (BUN) levels.

Hematoxylin and eosin (H&E) staining of kidney sections

Kidneys were collected at 24 h after the initiation of AKI and fixed with paraformaldehyde (4% in PBS), embedded in paraffin wax and sent to the University of Wisconsin Carbone Cancer Center Experimental Pathology Laboratory for sectioning and H&E staining.

Toxicity assessment *in vivo*

Toxicological analysis was carried out in 5-week-old healthy female ICR mice (Envigo, Indianapolis, IN, USA). Mice were randomized into three groups: Control, M13, and Rec-DON (n=10 for each group), which were injected with PBS (100 µL), M13 ssDNA (10 µg in 100 µL 1 x PBS), or Rec-DON (10 µg in 100 µL 1 x PBS), respectively. At 24 h after injection, all mice were euthanized. Whole blood samples were collected for hematology analysis (Abaxis VetScan HM5 Hematology Analyzer, USA). Major

organs (including the heart, liver, spleen, lung, and kidneys) from mice in the M13 and Rec-DON group were harvested for H&E staining to evaluate morphological changes and/or damage caused by administration of DNA materials.

Statistics

Quantitative data were displayed as the Mean ± Standard Deviation (SD). Statistical differences were determined using student t-test for two groups and one-way analysis of variance (ANOVA) for three and more groups. * (P values < 0.05), ** (P values < 0.01), and **** (P values <0.0001) were used to denote statistical significance. Statistical analysis was performed using GraphPad Prism7.00 (San Diego, CA, USA).

Supplementary Tables and Figures

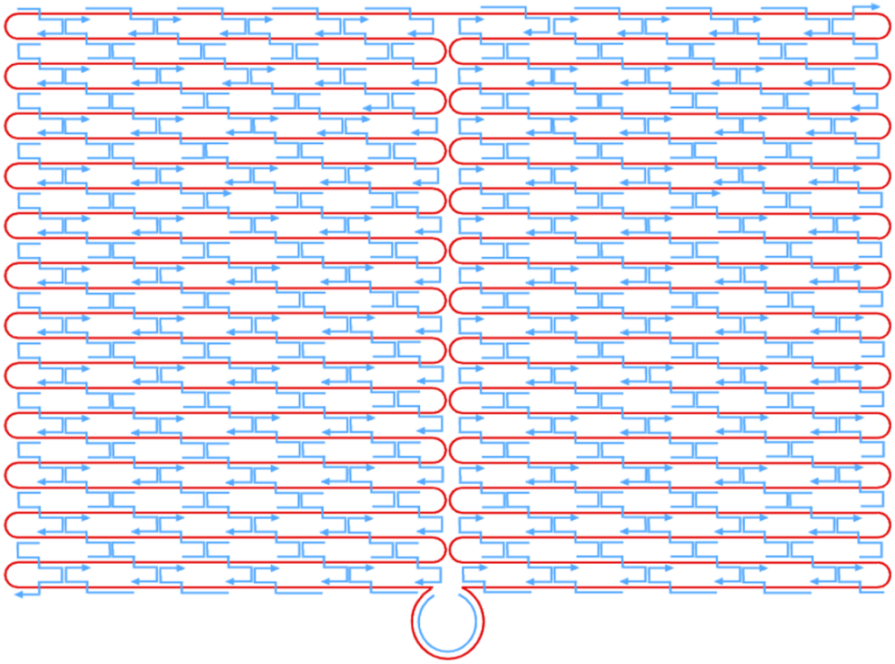

Figure S1. Schematic display of the folding strategy for rectangular DNA origami nanostructure (**Rec-DON**). Red line denotes M13; blue lines denote staple strands. Arrows denote direction from 5' to 3' for each DNA strand.

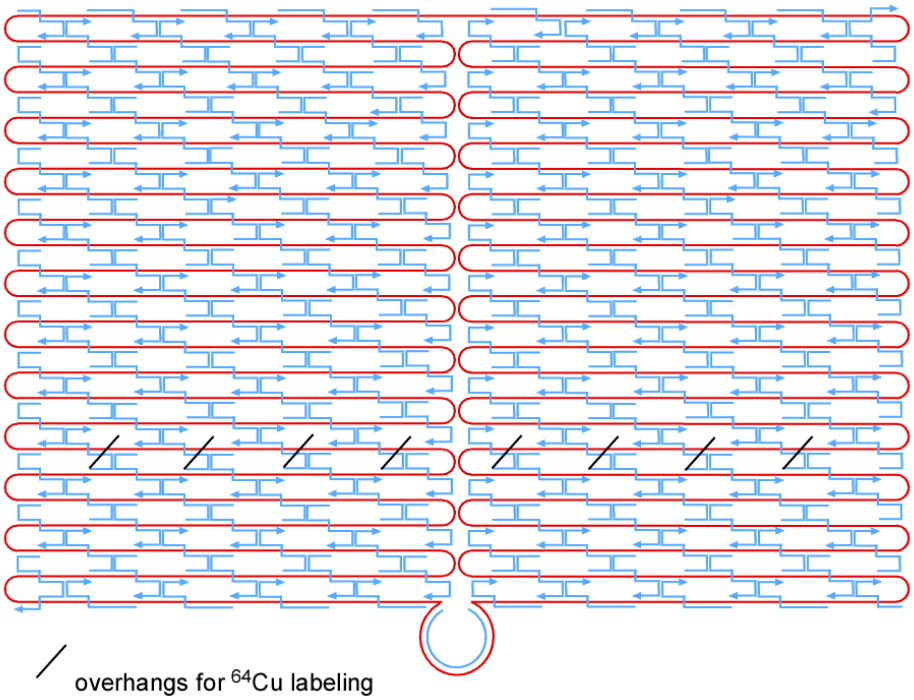

Figure S2. Schematic display of rectangular DNA origami nanostructure (Rec-DON) with eight overhangs. Red line denotes M13, blue lines denote staple strands, and black lines denote overhangs designed on the origami structure (to be hybridized with ^{64}Cu-labeled single-stranded DNA). Arrows denote direction from 5' to 3' for each DNA strand.

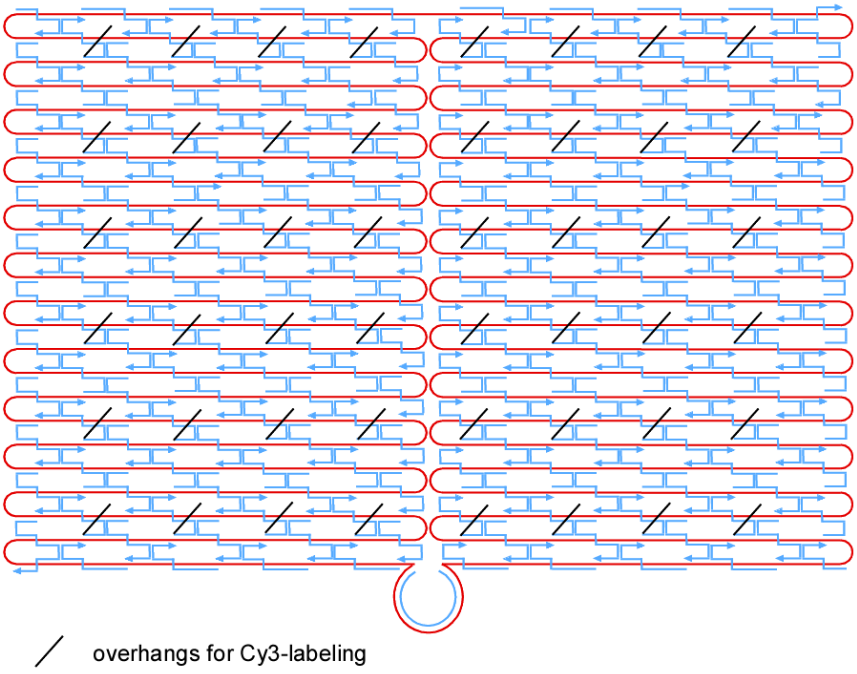

Figure S3. Schematic display of Rec-DON with 48 overhangs. Red line denotes M13, blue lines denote staple strands, and black lines denote overhangs (to be hybridized with Cy3-labeled single-stranded DNA). Arrows denote direction from 5' to 3' for each DNA strand.

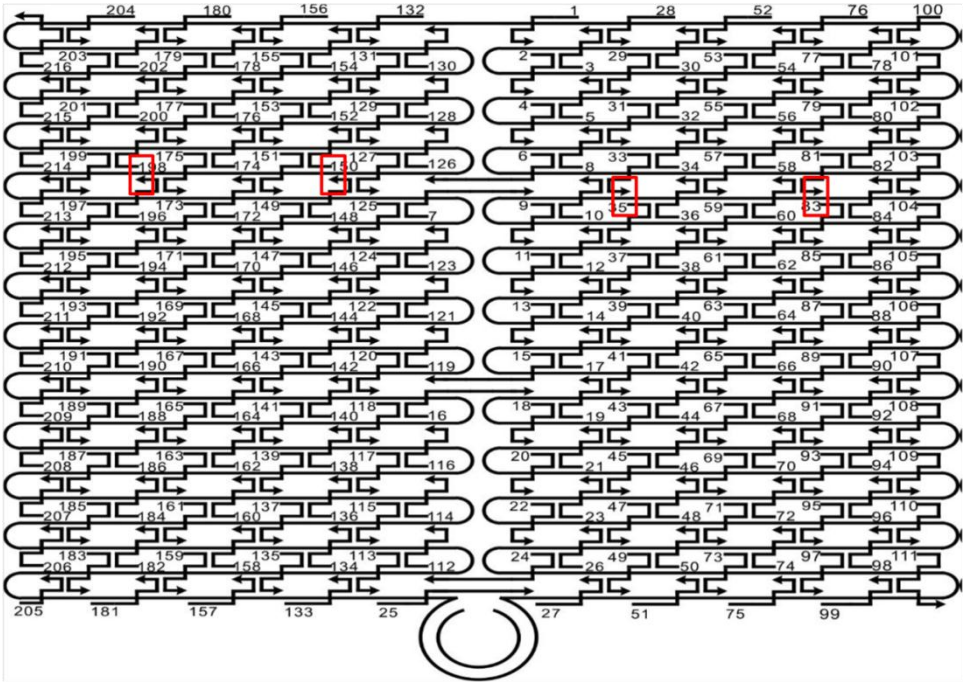

Figure S4. Schematic display of Cy3/Cy5 dual-labeled Rec-DON. Staple strands 198, 150, 33, and 81 have been labeled with Cy5 on 5'-end, and strands 196, 148, 35, and 83 have been labeled with Cy3 on 3’-end. Red rectangles indicated the positions of the four FRET pairs on a Rec-DON structure. Arrows denote direction from 5’ to 3’ for each DNA strand.

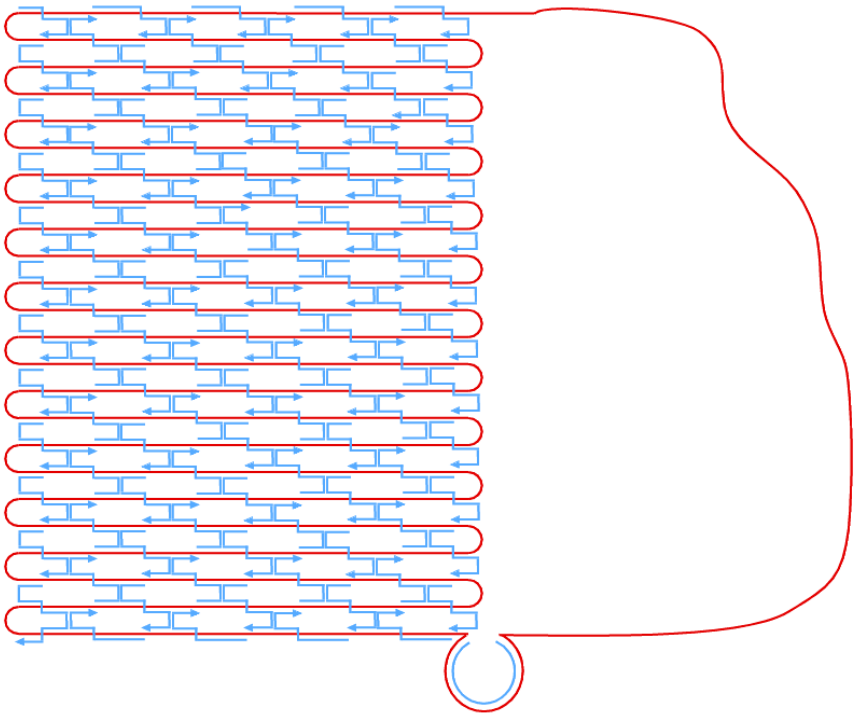

Figure S5. Schematic display of the folding strategy for the partially-folded Rec-DON. Red line denotes M13; blue lines denote staple strands. Arrows denote direction from 5’ to 3’ for each DNA strand.

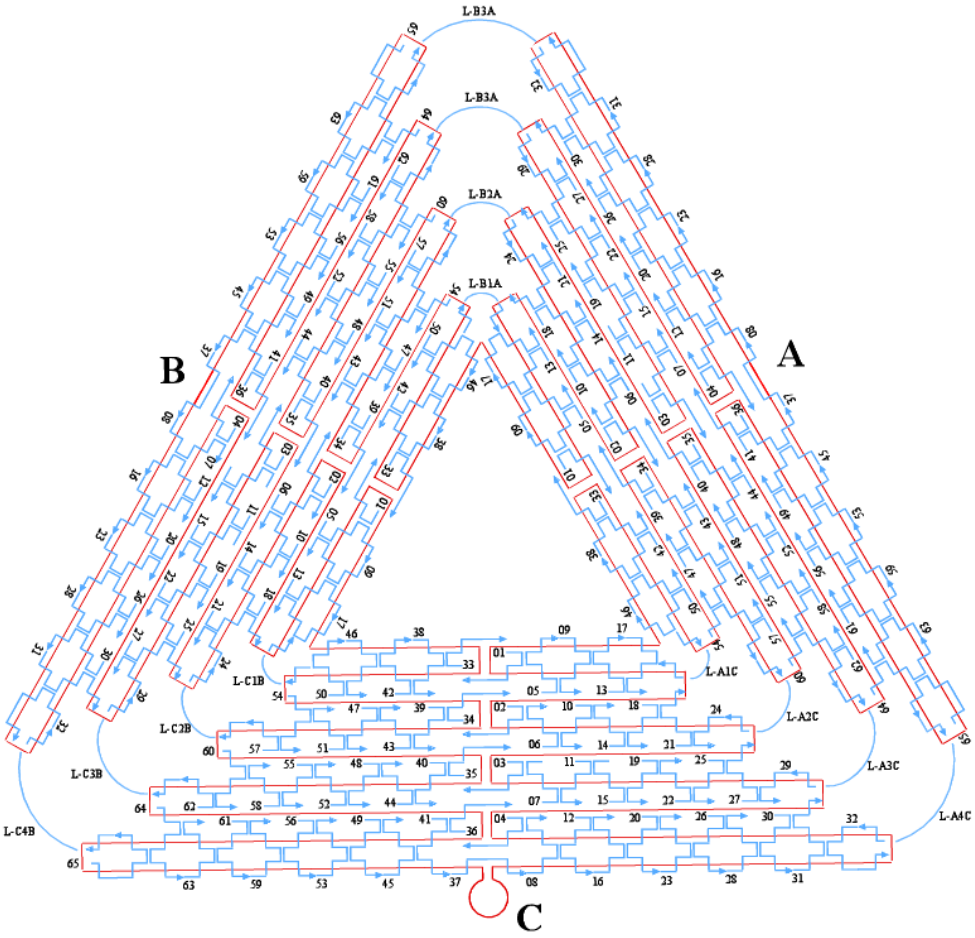

Figure S6. Schematic display of the folding strategy for triangular DNA origami nanostructures (**Tri-DON**). Red line denotes M13; blue lines with numbers denote staple strands. Arrows denote direction from 5' to 3' for each DNA strand.

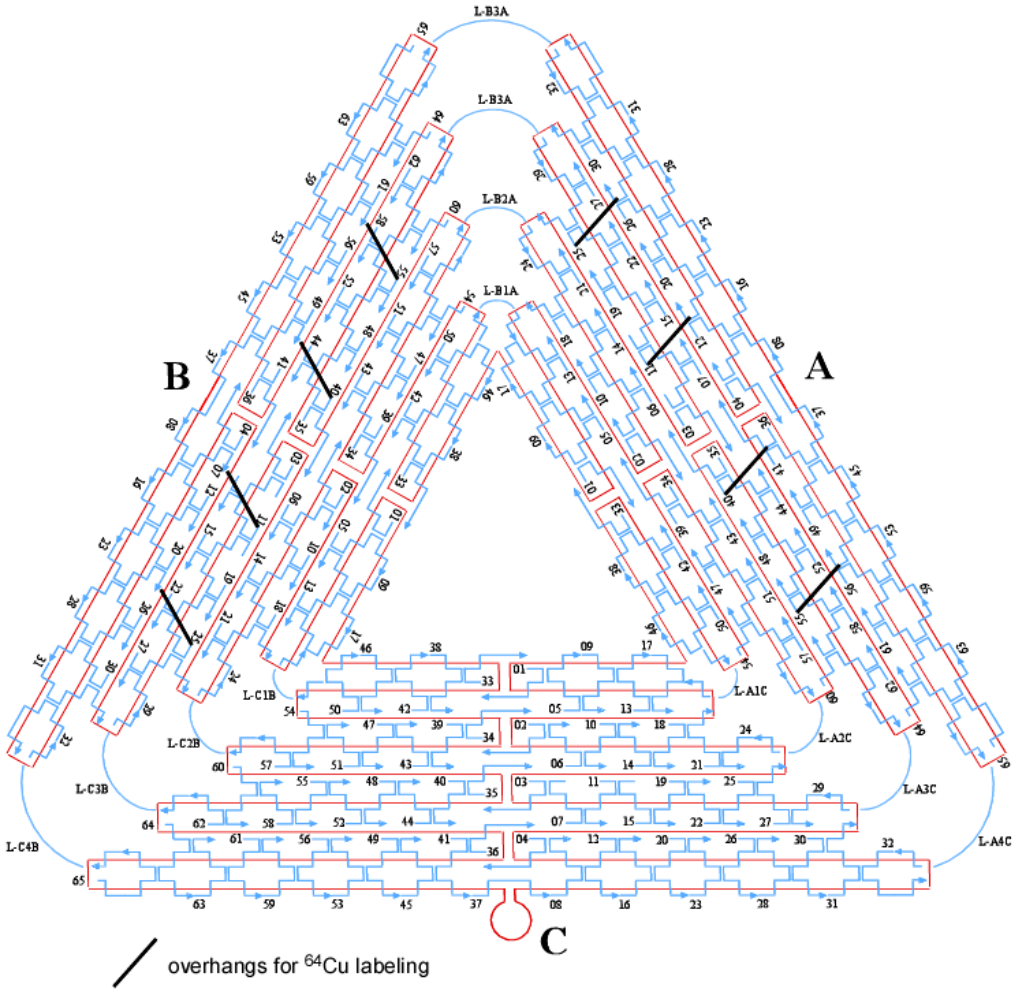

Figure S7. Schematic display of Tri-DON with eight overhangs. Red line denotes M13, blue lines with numbers denote staple strands, and black lines denote overhangs designed on Tri-DON (to be hybridized with ^{64}Cu-labeled single-stranded DNA). Arrows denote direction from 5' to 3' for each DNA strand.

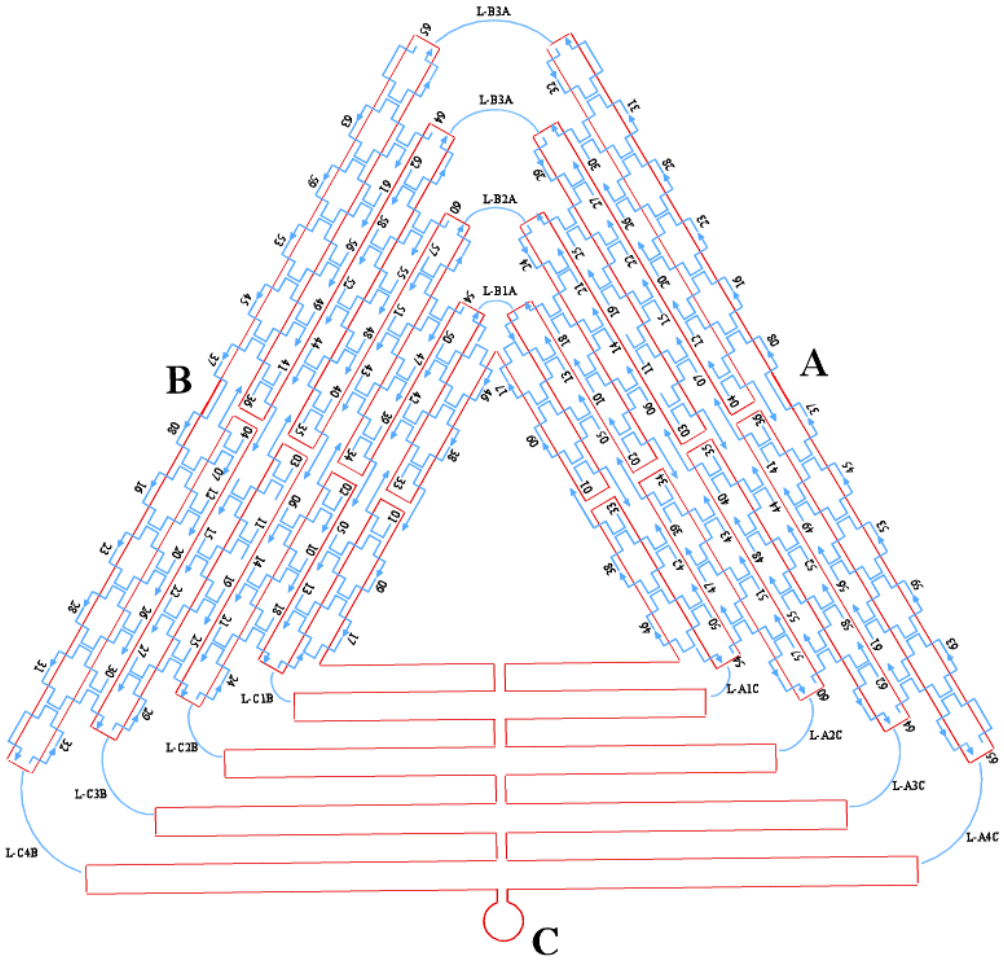

Figure S8. Schematic display of partially-folded Tri-DON. Red line denotes M13, blue lines with numbers denote staple strands. Arrows denote direction from 5’ to 3’ for each DNA strand.

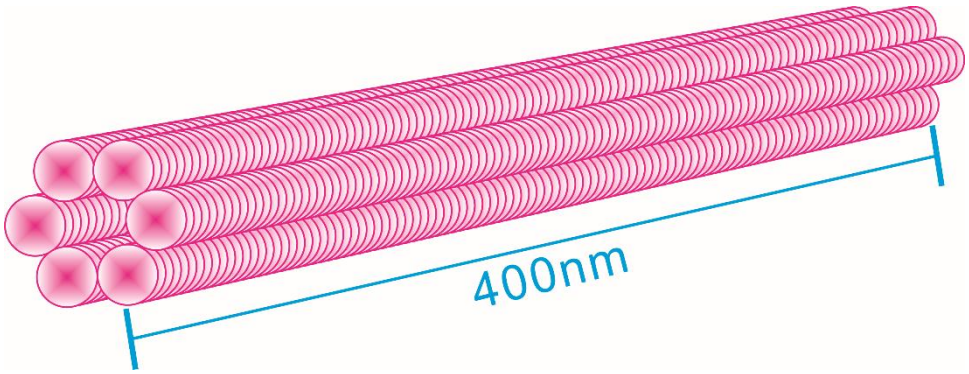

Figure S9. Schematic display of tubular DNA origami (**Tub-DON**).

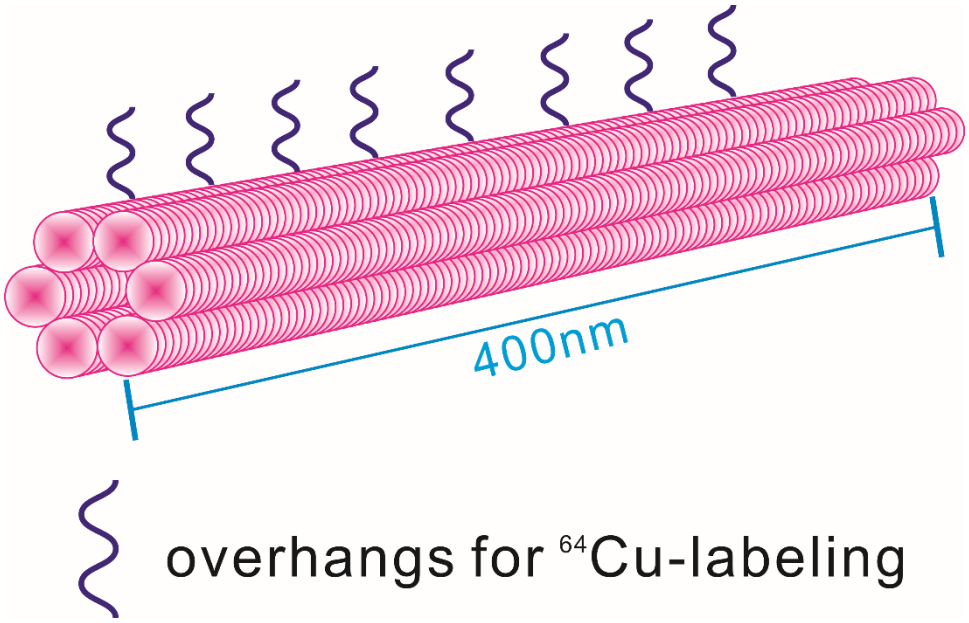

Figure S10. Schematic display of tubular DNA origami (Tub-DON) with eight overhangs. Magenta tubes denote tubular DNA origami; blue curves denote eight overhangs designed on Tub-DON.

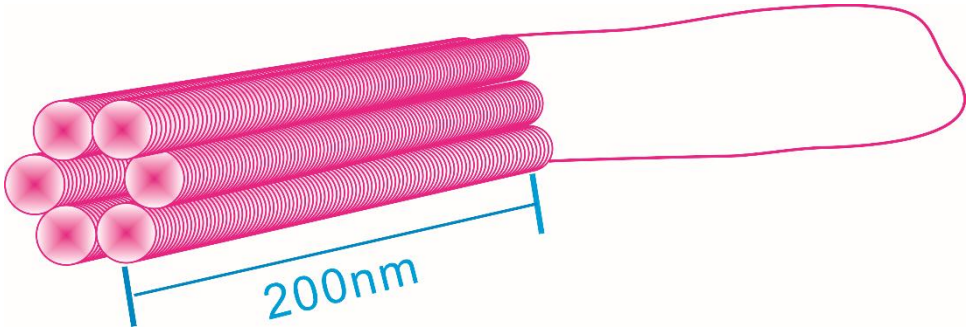

Figure S11. Schematic display of partially-folded Tub-DON.

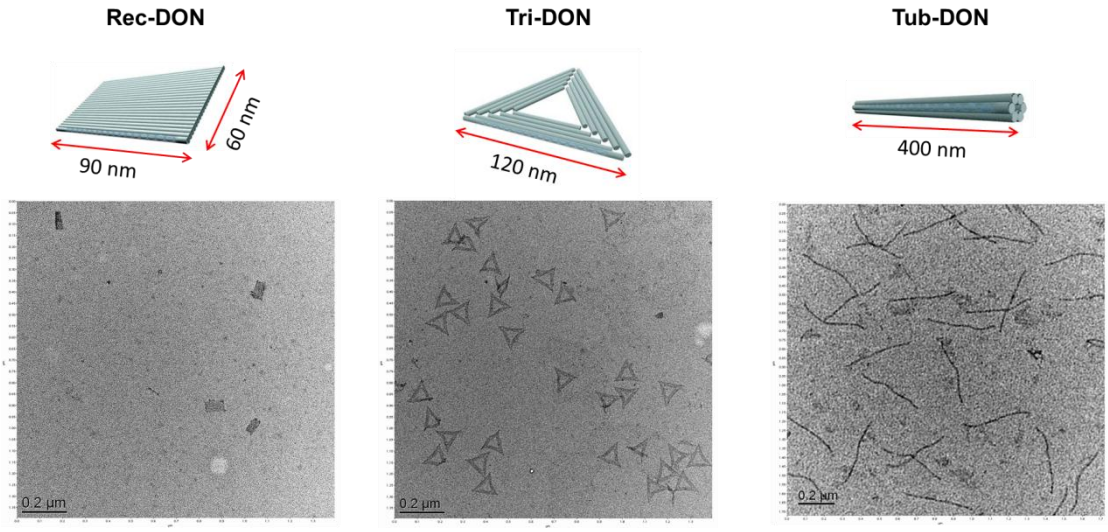

Figure S12. Representative TEM images of DNA origami nanostructures after negative staining. Scale bar: 200 nm. One of three independent experiments was shown.

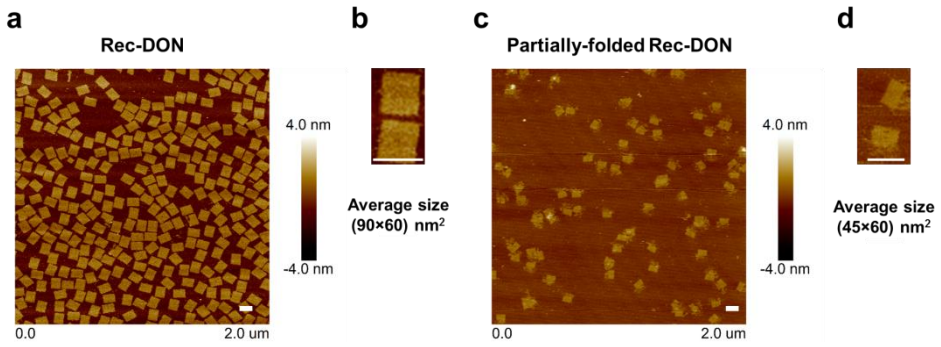

FigureS13. Representative AFM images of fully-folded Rec-DON (**a**) and partially-folded Rec-DON (**c**). Panel (**b)** and (**d)** showed magnified images of two DNA origami nanostructures, the size of intact Rec-DON was approximately 90 x 60 nm, and partially-folded Rec-DON was approximately 45 x 60 nm. Scale bar: 100 nm. One of three independent experiments was shown.

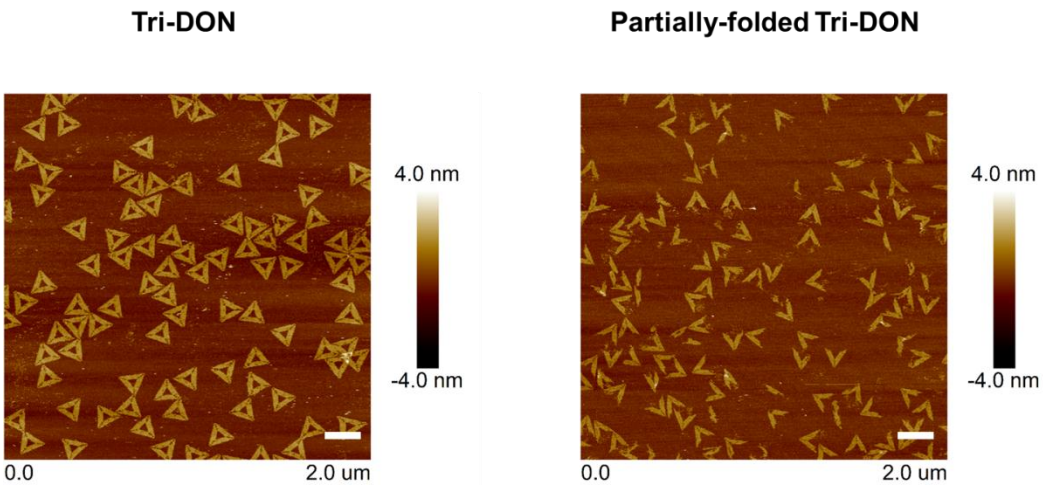

Figure S14. Representative AFM images of fully-folded Tri-DON (left) and partially-folded Tri-DON (right). Scale bar: 200 nm. One of three independent experiments was shown.

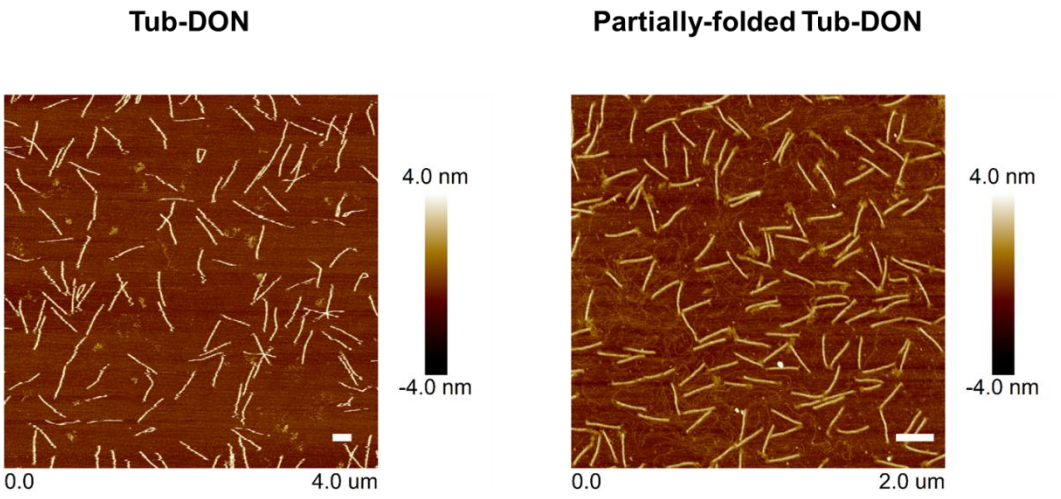

Figure S15. Representative AFM images of fully-folded Tub-DON (left) and partially-folded Tub-DON (right). Scale bar: 200 nm. One of three independent experiments was shown.

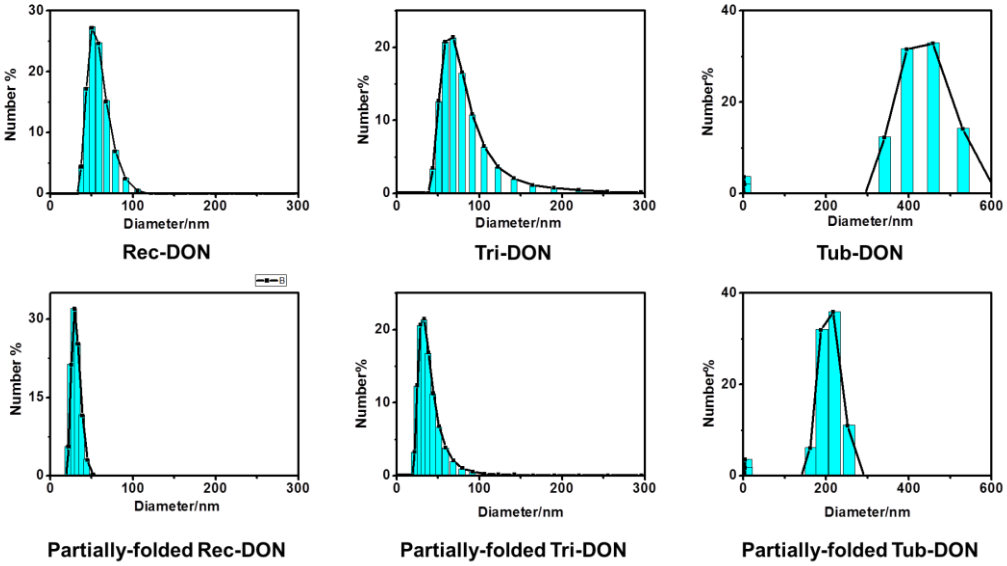

Figure S16. Hydrodynamic diameters of intact or partially-folded DONs measured by dynamic light scattering (DLS). Each column represents the mean value of 11 measurements as default settings of the DLS workstation.

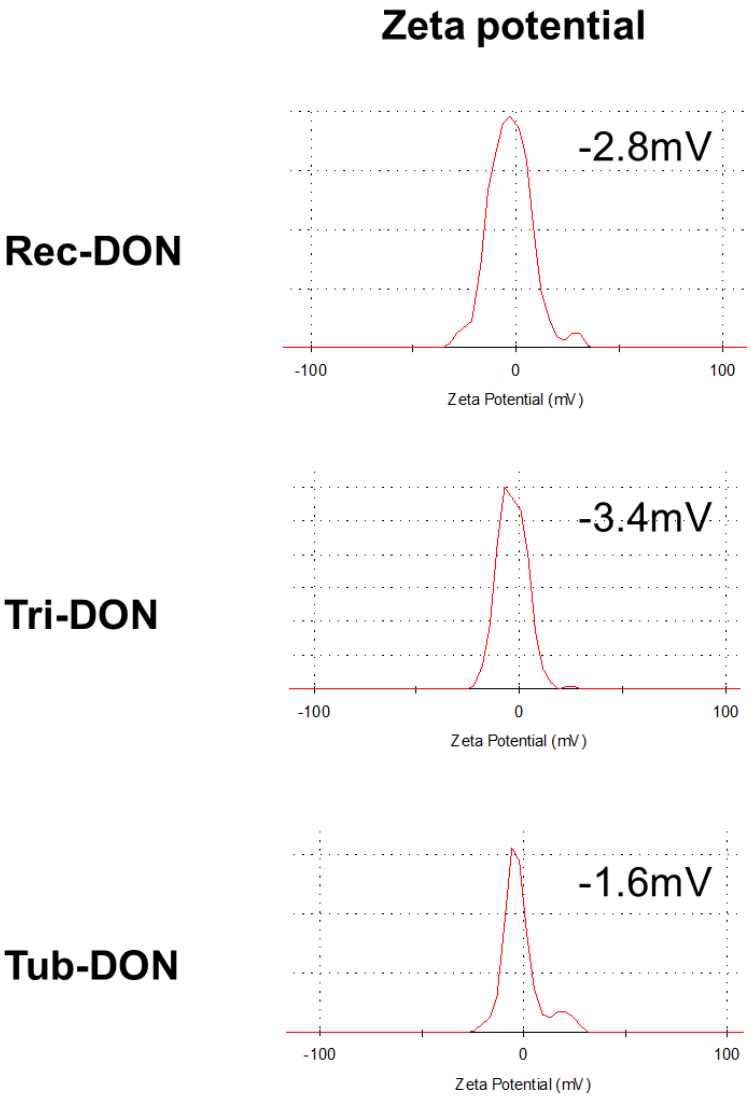

Figure S17. Zeta potential of intact DONs. One of three independent experiments was shown.

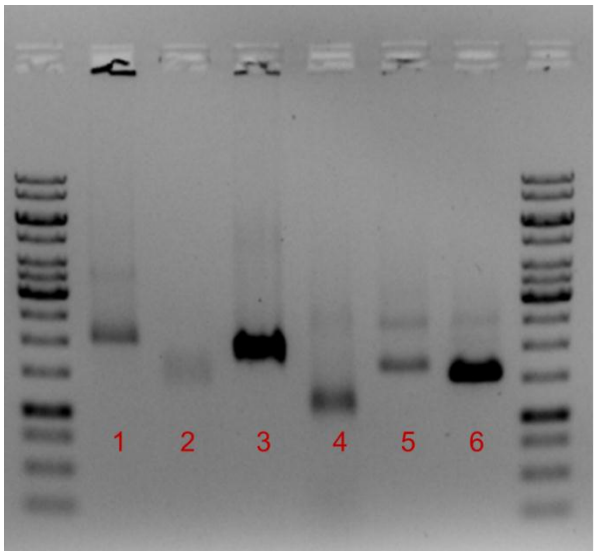

1. Tri-DON
2. Partially-folded Tri-DON
3. Tub-DON
4. Partially-folded Tub-DON
5. Rec-DON
6. Partially-folded Rec-DON

Figure S18. Agarose gel electrophoresis (AGE) of intact or partially-folded DONs. One of three independent experiments was shown.

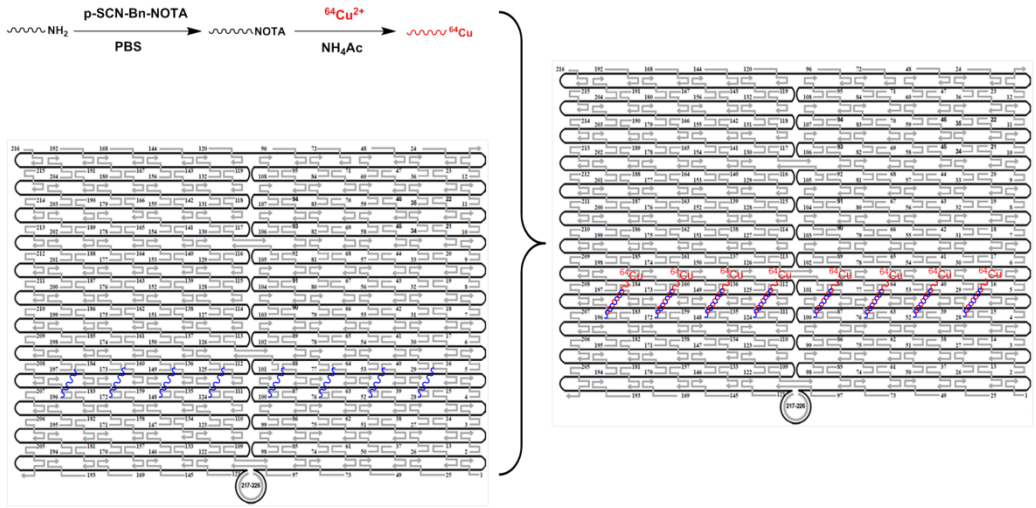

Figure S19. ^{64}Cu-labeling of DONs (Rec-DON was used as an example in this figure). Eight overhangs were designed on DONs. After labeling of DNA strands with ^{64}Cu to obtain ^{64}Cu-ssDNA, DON was then mixed with ^{64}Cu-ssDNA for hybridization to prepare ^{64}Cu-labeled DONs.

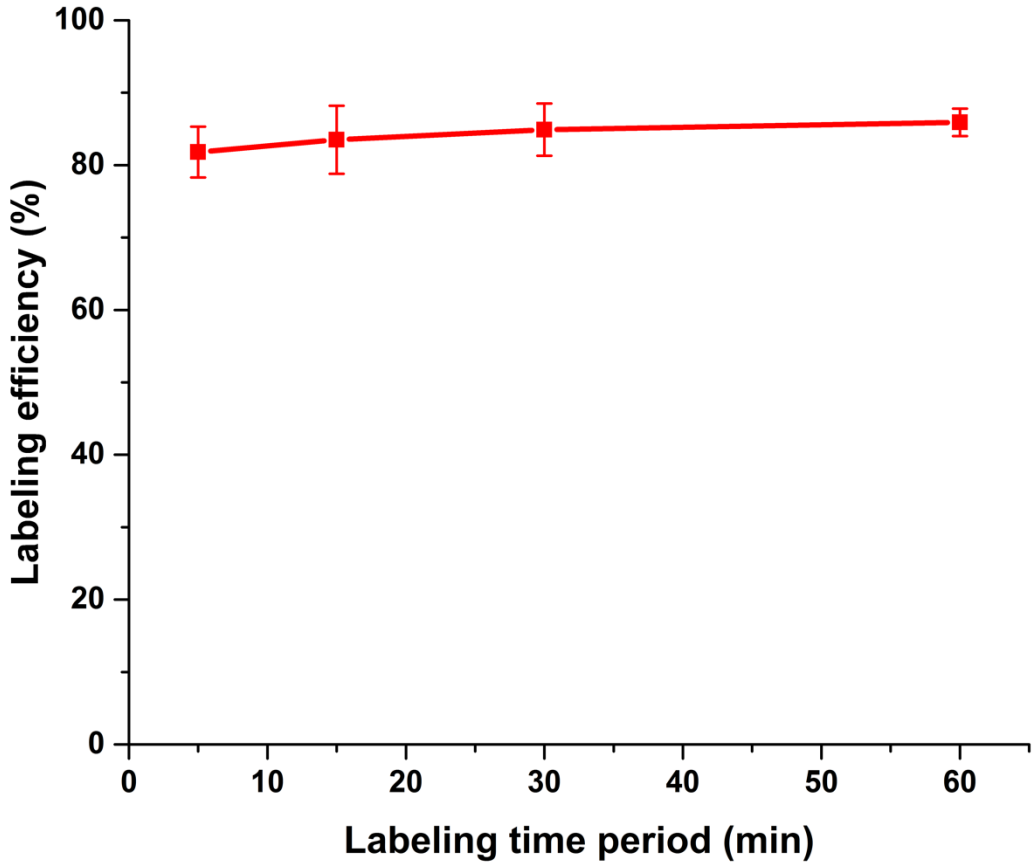

Figure S20. Time dependent radiolabeling yield of ssDNA with ^{64}Cu (n=5). Data represent mean ± standard deviation.

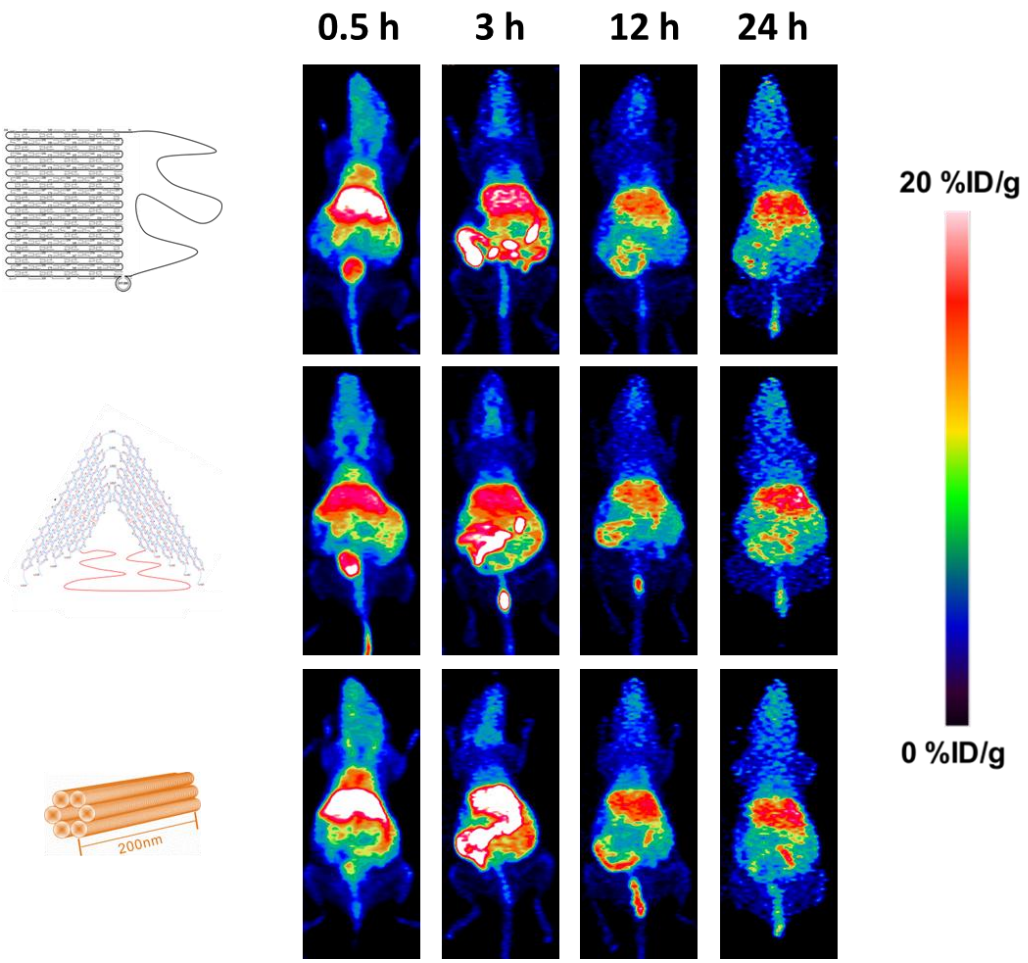

Figure S21. Maximum intensity projection (MIP) PET images of ^{64}Cu-labeled partially-folded DNA origami nanostructures in healthy ICR mice (n=3 for each structure). First row: partially-folded Rec-DON; second row: partially-folded Tri-DON; third row: partially-folded Tub-DON.

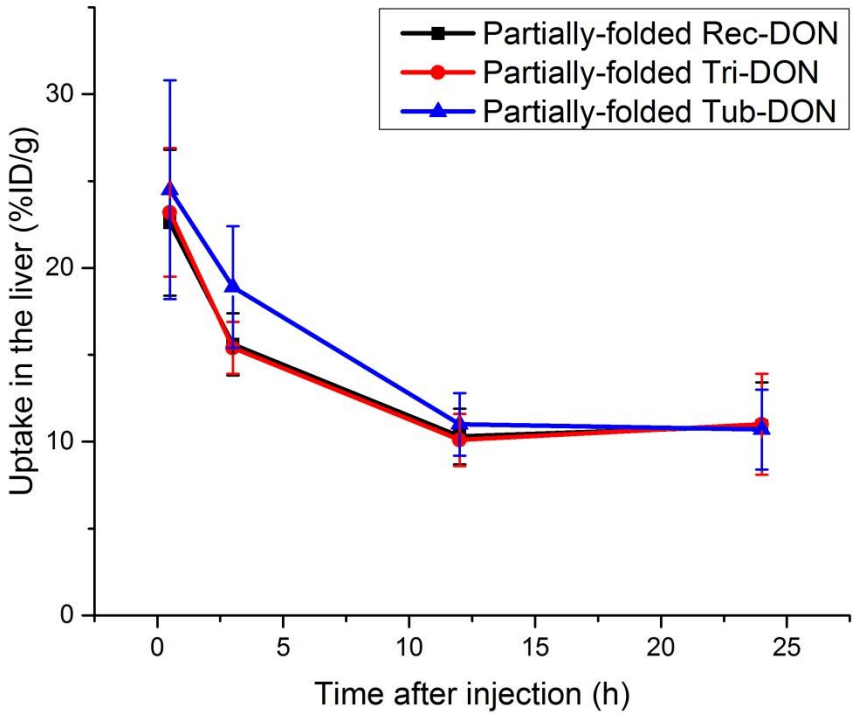

Figure S22. ROI analysis of the liver after *i.v.* injection of ^{64}Cu-labeled partially-folded DONs into healthy ICR mice. n=3. Data represent mean ± standard deviation.

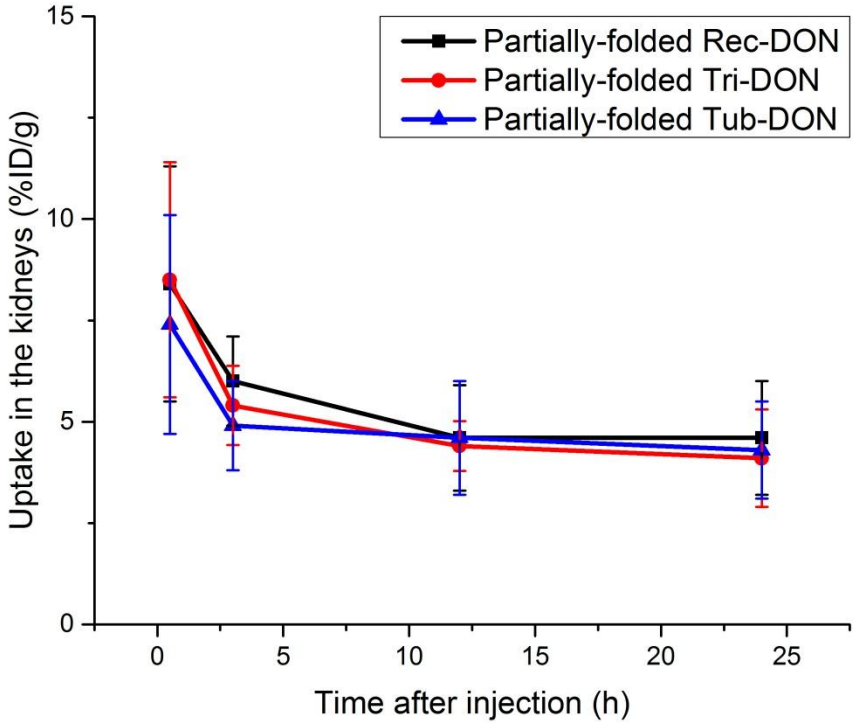

Figure S23. ROI analysis of the kidneys after *i.v.* injection of ^{64}Cu-labeled partially-folded DONs into healthy ICR mice. n=3. Data represent mean ± standard deviation.

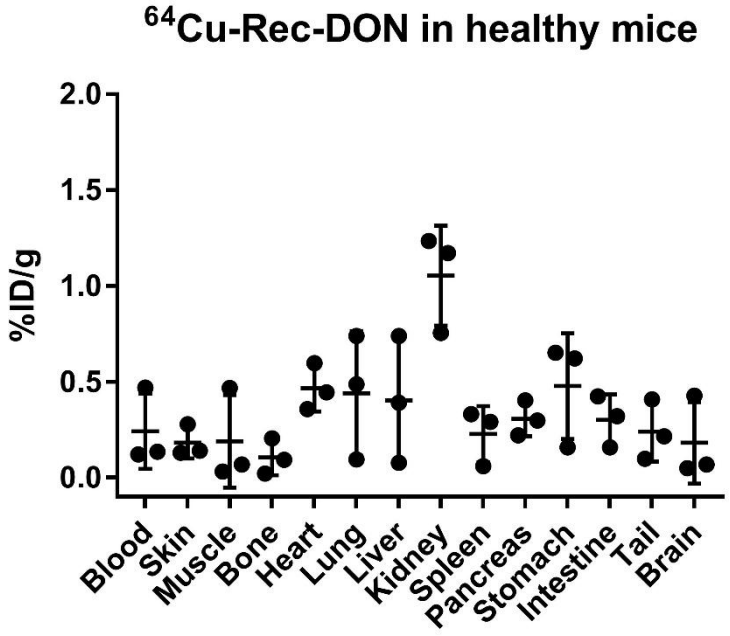

Figure S24. Biodistribution of ^{64}Cu-labeled Rec-DON in healthy mice at 24 h after injection. n=3. Data represent mean ± standard deviation.

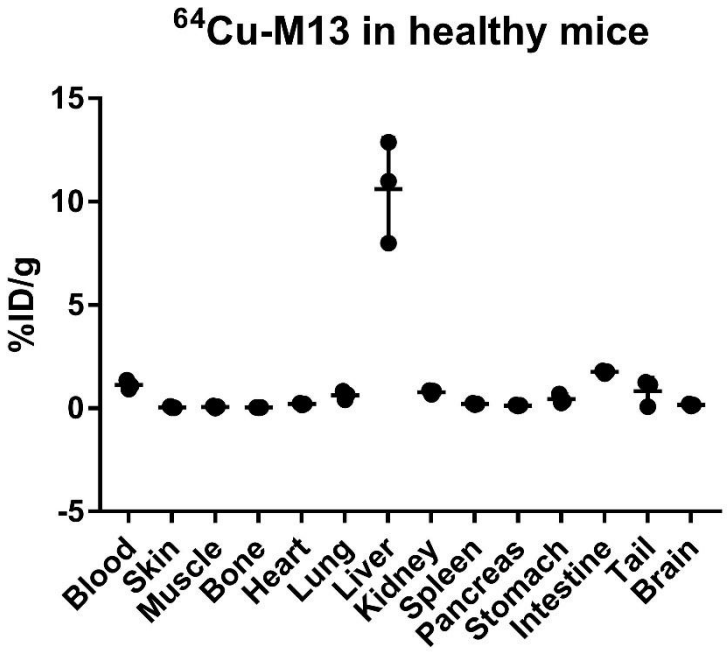

Figure S25. Biodistribution of ^{64}Cu-labeled M13 in healthy mice at 24 h after injection. n=3. Data represent mean ± standard deviation.

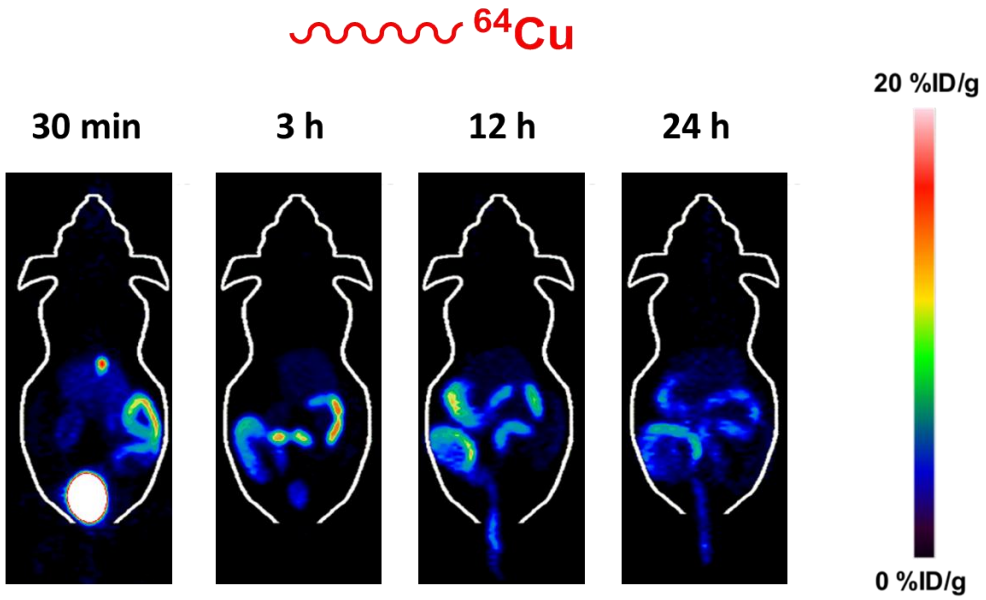

Figure S26. Maximum intensity projection (MIP) PET images of ^{64}Cu-ssDNA in healthy mice at various time points after injection. n=3.

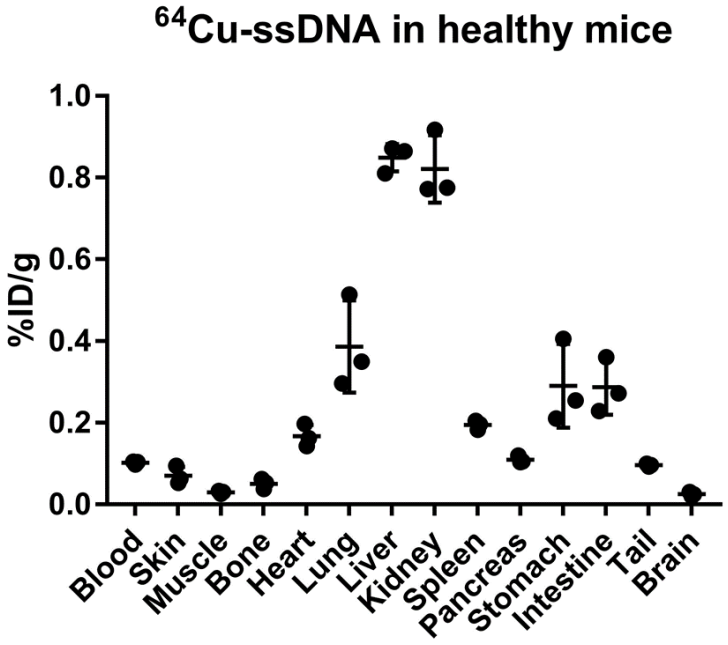

Figure S27. Biodistribution of ^{64}Cu-labeled ssDNA in healthy mice at 24 h after injection. n=3. Data represent mean ± standard deviation.

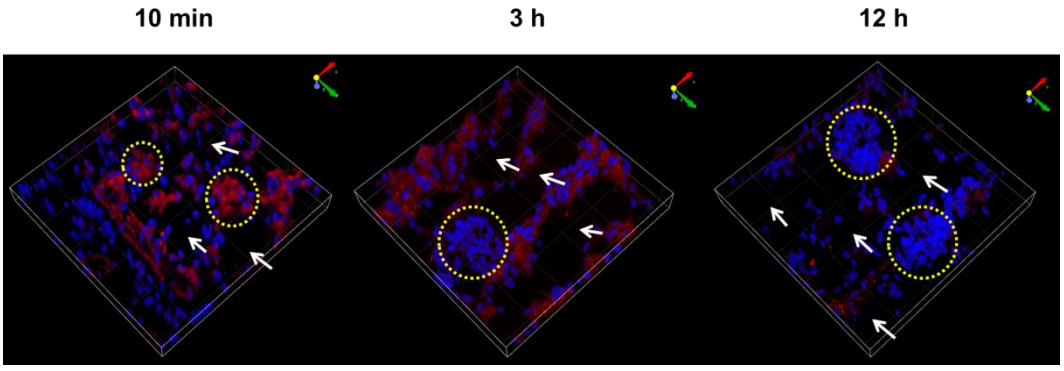

Figure S28. Confocal imaging of kidney tissue sections. One of three independent experiments was shown. Mice were injected with Cy3-Rec-DON (red) and kidneys were harvested at 10 min, 3 h, and 12 h after injection. Blue: DAPI for nuclear staining. Dashed yellow circles denote the glomeruli and white arrows denote renal tubular lumina. Field of view: 100 x 100 µm.

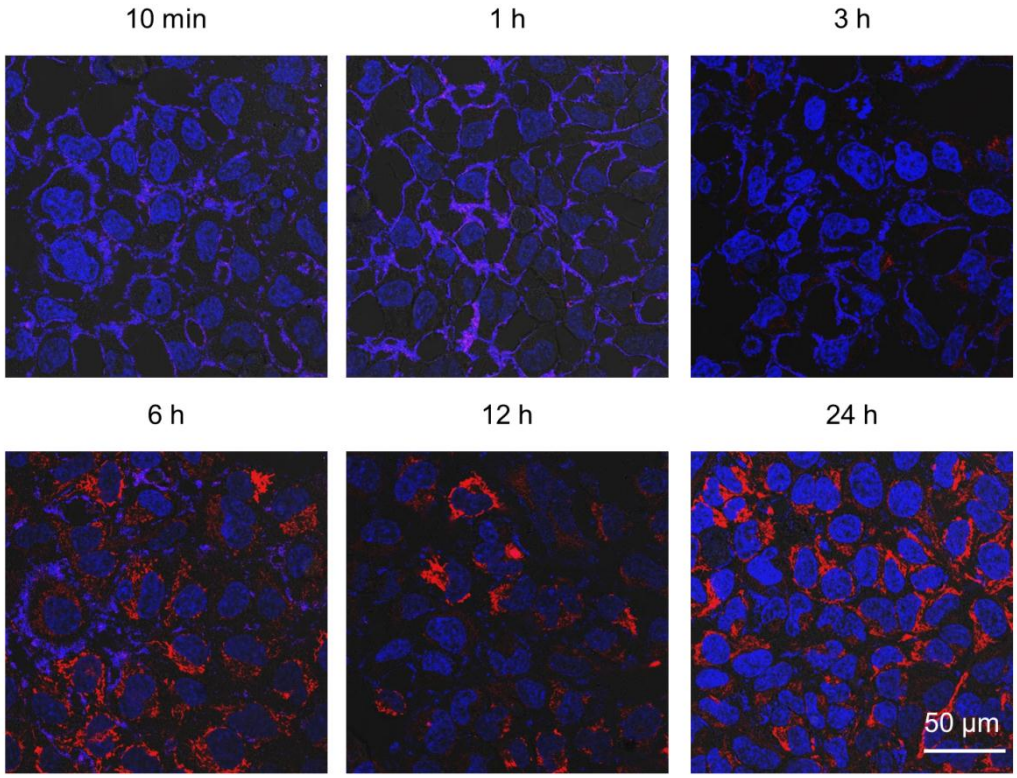

Figure S29. Cell internalization study of Cy3-labeled Rec-DON using HEK293 cells. Blue color (Hoechst) represents the nuclei; red color stands for Cy3-labeled Rec-DON. One of three independent experiments was shown.

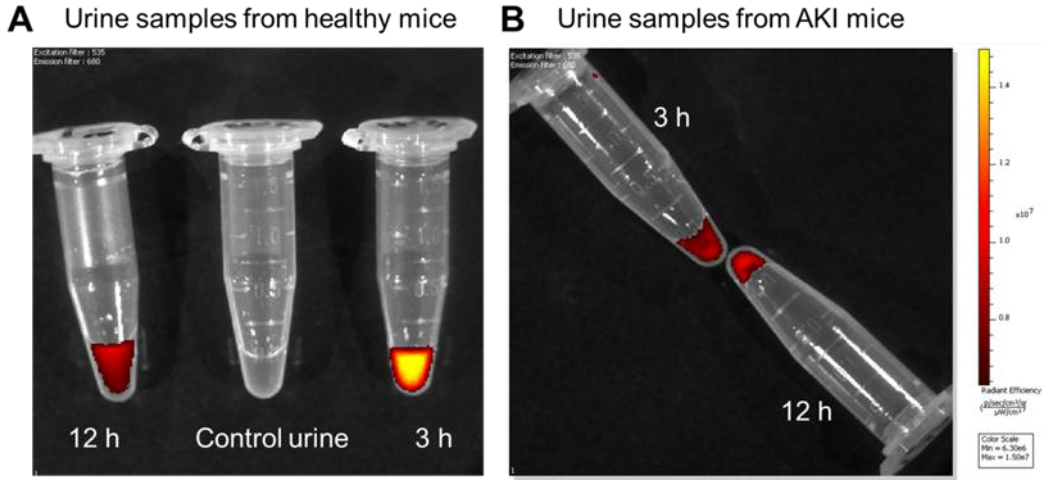

Figure S30. **(A)** Fluorescence resonance energy transfer (FRET) of healthy mouse urine collected at 3 h and 12 h after *i.v.* injection of FRET Rec-DON (i.e. Cy3/Cy5 dual-labeled). Clean urine was used as a control sample (Ex/Em= 535/680 nm, which detects the FRET signal with excitation of Cy3 and emission of Cy5). One of three independent experiments was shown. **(B)** FRET of AKI mouse urine collected at 3 h and 12 h after injection of FRET Rec-DON (Ex/Em= 535/680 nm, as shown in the upper-left corner of the image). One of three independent experiments was shown.

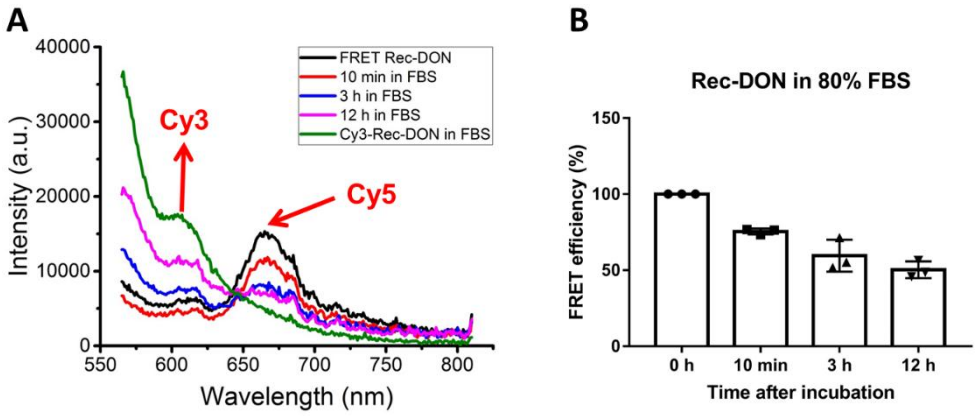

Figure S31. (A) Fluorescence resonance energy transfer (FRET) of Cy3/Cy5 dual-labeled Rec-DON in 80% FBS. Cy3-labeled Rec-DON was used as a control sample. One of three independent experiments was shown. (B) FRET efficiencies of Cy3/Cy5 dual-labeled Rec-DON in 80% FBS at 0 min, 10 min, 3 h, and 12 h, respectively. n=3. Data represent mean ± standard deviation.

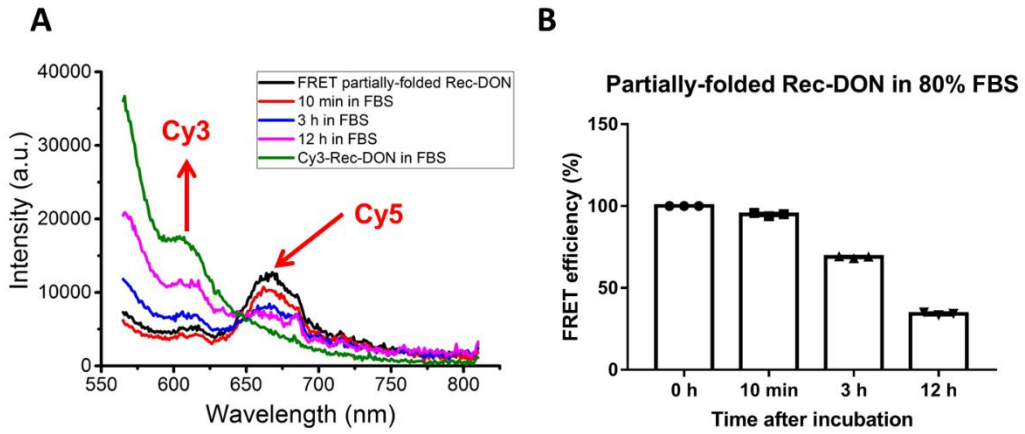

Figure S32. (A) Fluorescence resonance energy transfer (FRET) of Cy3/Cy5 dual-labeled partially-folded Rec-DON in 80% FBS. Cy3-labeled Rec-DON was used as a control sample. One of three independent experiments was shown. (B) FRET efficiencies of Cy3/Cy5 dual-labeled Rec-DON in 80% FBS at 0 min, 10 min, 3 h, and 12 h, respectively. n=3. Data represent mean ± standard deviation.

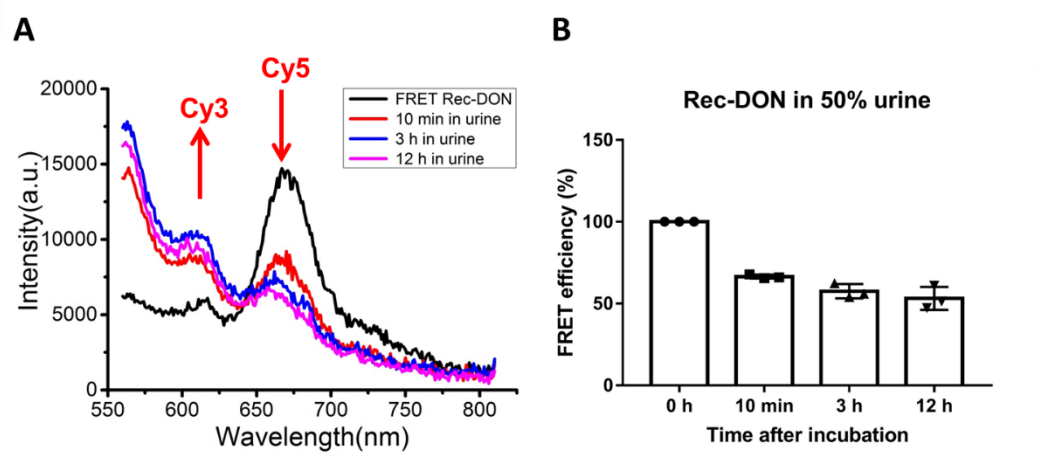

Figure S33. (A) Fluorescence resonance energy transfer (FRET) of Cy3/Cy5 dual-labeled Rec-DON in 50% mouse urine. One of three independent experiments was shown. (B) FRET efficiencies of Cy3/Cy5 dual-labeled Rec-DON in 50% mouse urine at 0 min, 10 min, 3 h, and 12 h, respectively. n=3. Data represent mean ± standard deviation.

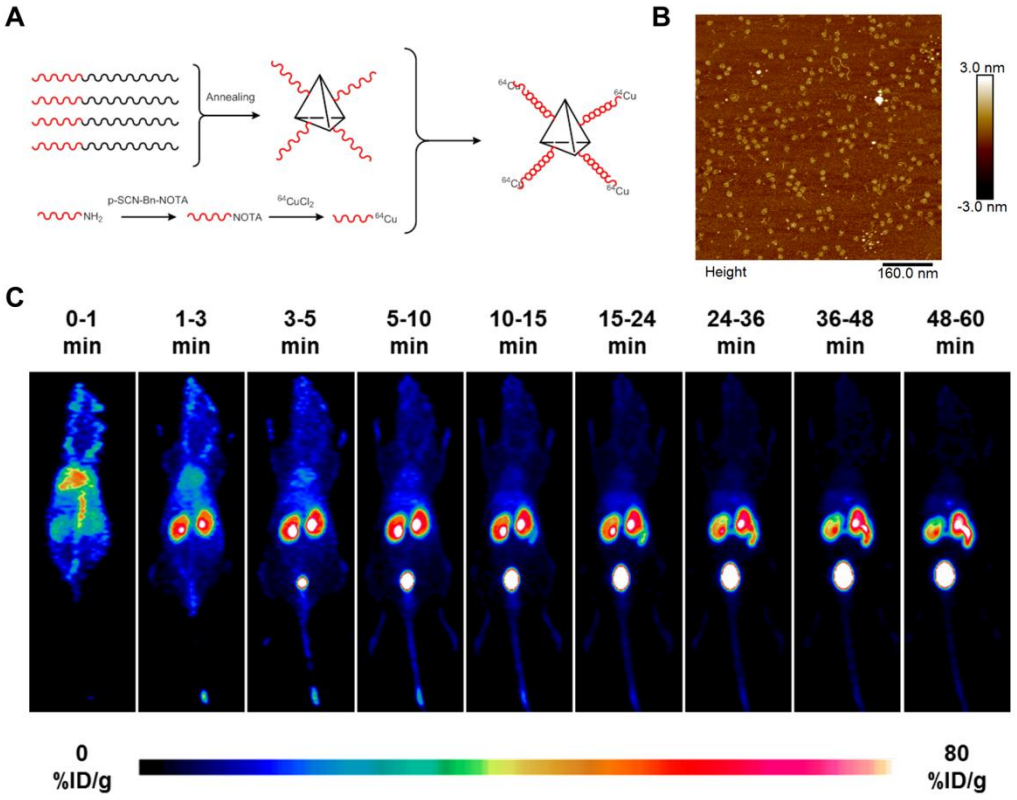

Figure S34. Biodistribution study of DNA tetrahedron nanoparticle (DTN) in healthy mice. (A) Schematic display of the assembly and radiolabeling process of DTN to obtain ^{64}Cu-DTN. (B) AFM imaging of DTN. One of three independent experiments was shown. (C) PET images of healthy mice after intravenous injection of ^{64}Cu-DTN (representative of a group of 3 mice).

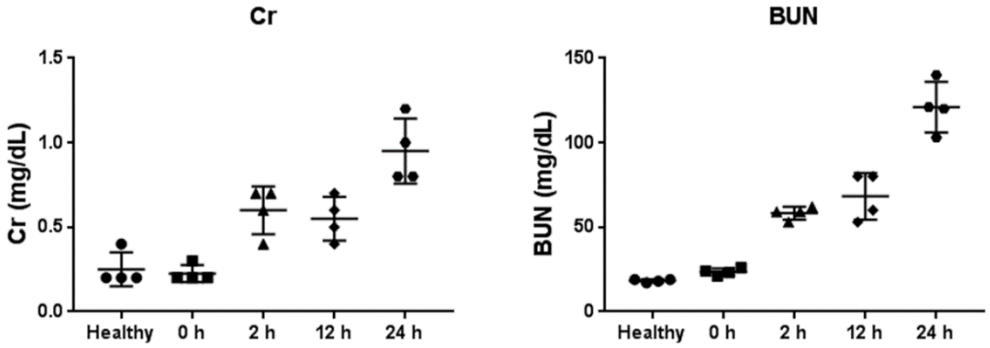

Figure S35. Analysis of serum creatinine (Cr, Left) and blood urea nitrogen (BUN, right) levels of AKI mice after model initiation. Lower levels of Cr and BUN indicate better kidney functions. n=4 for each group. Data represent mean ± standard deviation.

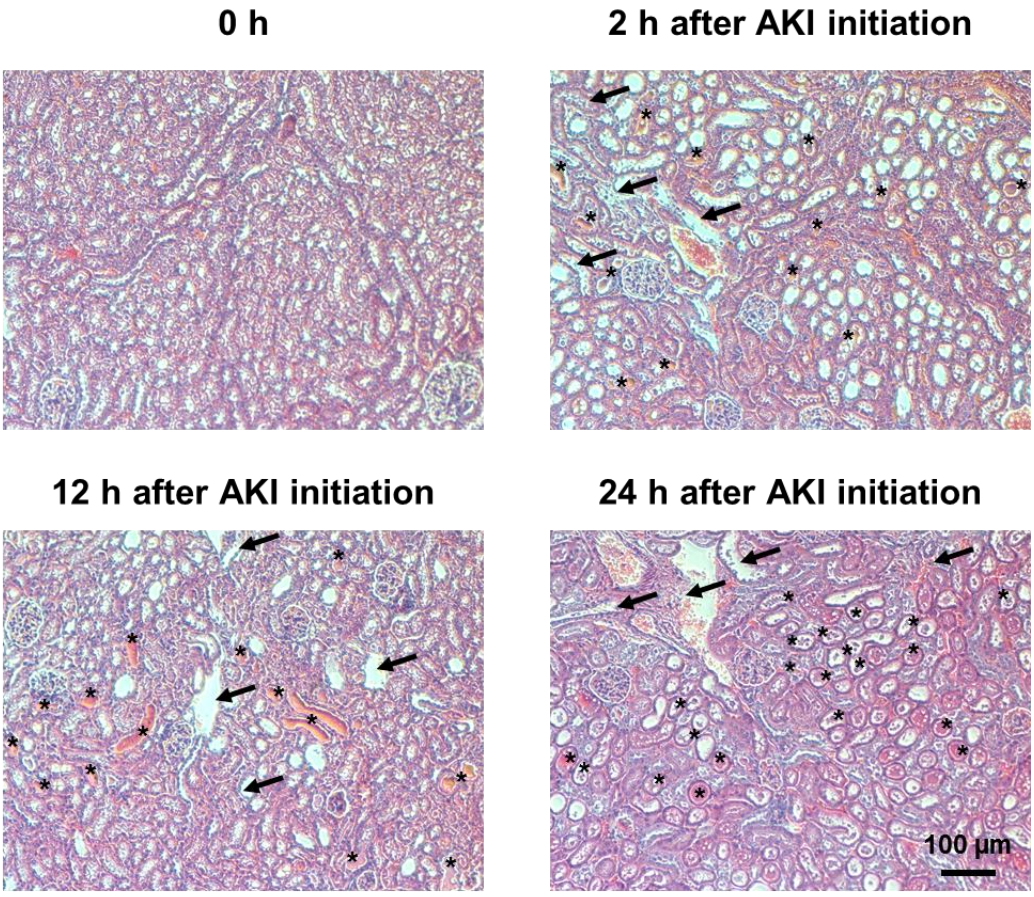

Figure S36. H&E staining of kidney tissues of AKI mice at different time points after model initiation. Arrows denote damaged tubules, and asterisks denote the formation of casts, a structure formed via precipitation of denatured proteins in the tubules. Scale bar: 100 μm. One of three independent experiments is shown.

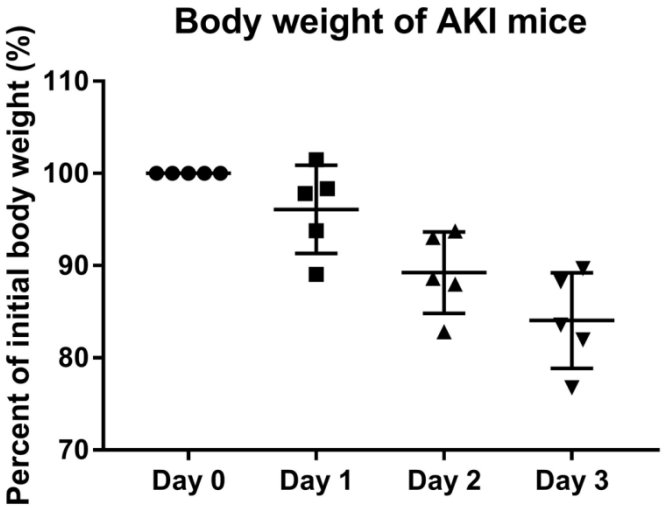

Figure S37. Changes of mouse body weight within 3 days after AKI model initiation.

At Day 3, all mice died from AKI. n=5. Data represent mean ± standard deviation

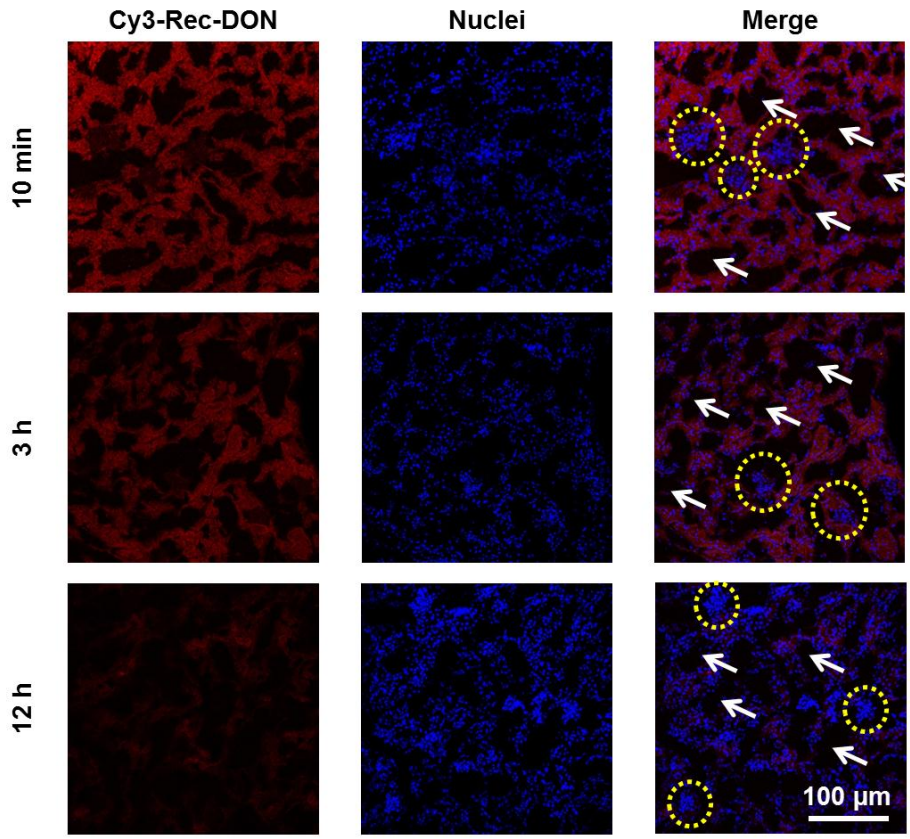

Figure S38. Confocal images of kidney sections after *i.v.* injection of Cy3-labeled Rec-DON (red signal) in AKI mice. Nuclei were stained with 2-(4-amidinophenyl)-1H-indole-6-carboxamidine (DAPI, blue). Yellow dashed circles denote the glomerulus, and white arrows denote renal tubular lumina. Scale bar: 100 μm. One of three independent experiments is shown.

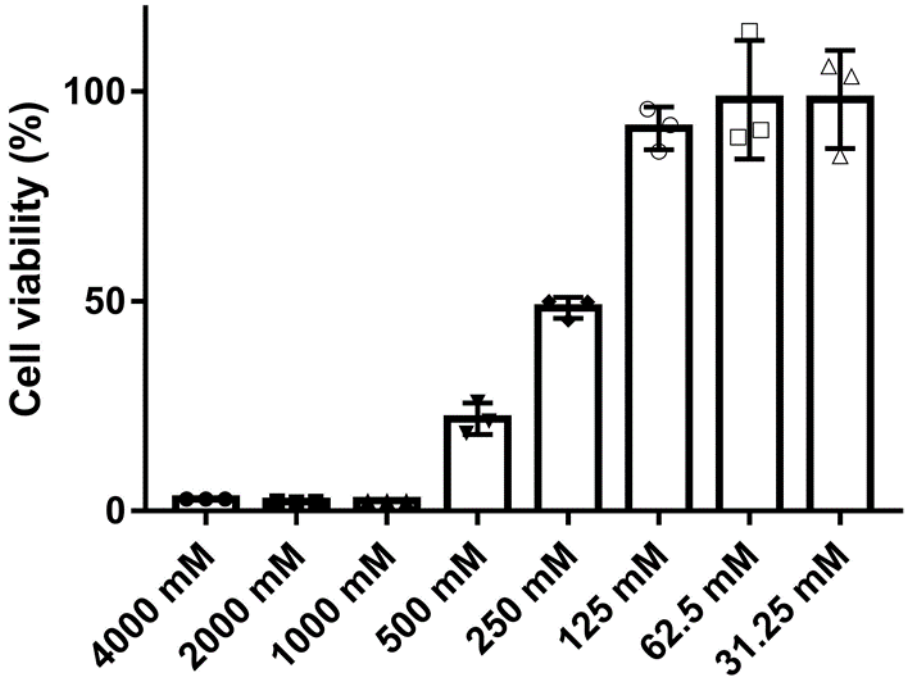

Figure S39. Cell viability assay using HEK293 cells incubating with different concentrations of H_2O_2. n=3. Data represent mean ± standard deviation.

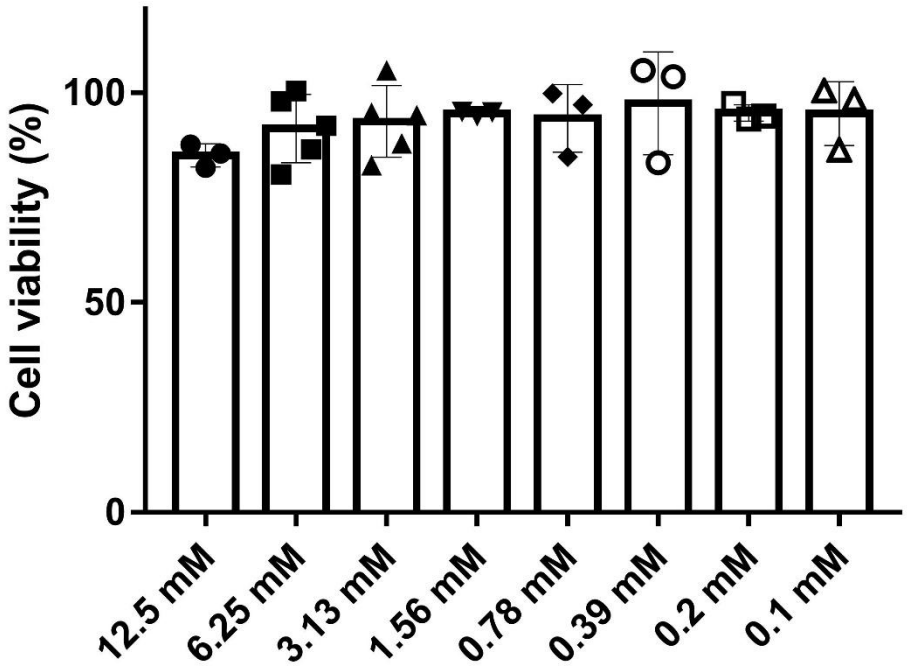

Figure S40. Cell viability assay using HEK293 cells incubating with different concentrations of Mg^{2+}. n=5 for Group 6.25 mM and 3.13 mM, n=3 for all other groups. Data represent mean ± standard deviation.

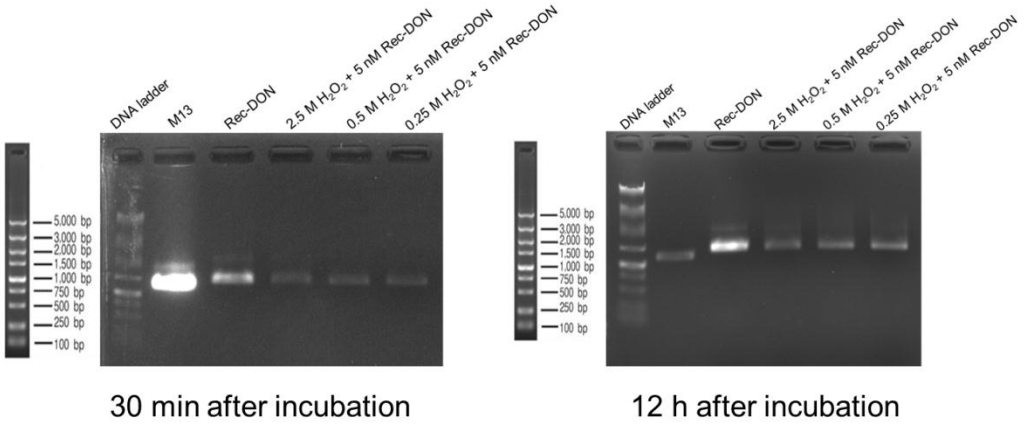

Figure S41. Agarose gel electrophoresis of Rec-DON (5 nM) incubated in different concentration of H_2O_2 for 30 min (left) and 12 h (right), which showed no sign of disassembly. M13 and Rec-DON were added as controls. One of three independent experiments is shown.

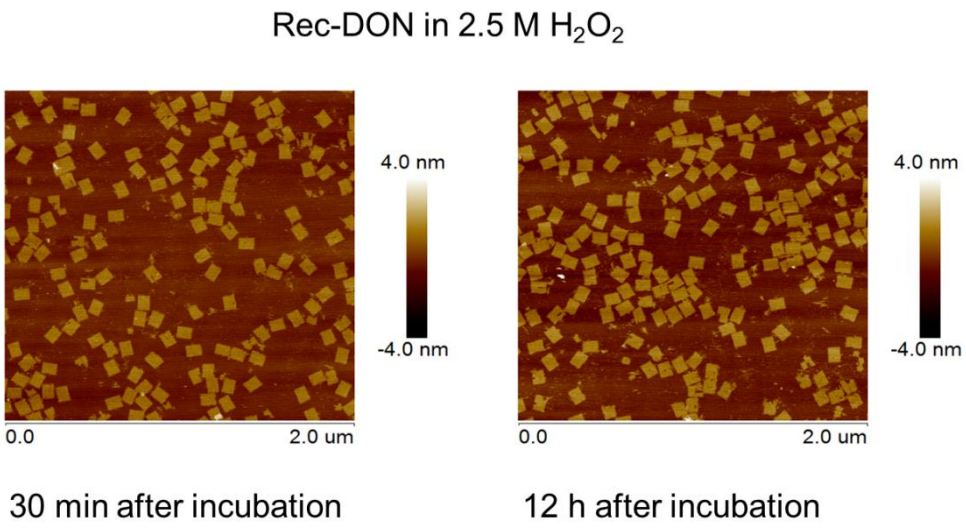

Figure S42. AFM images of Rec-DON (5 nM) after incubation in H_2O_2 (2.5 M) for 30 min (left) and 12 h (right) and we found no significant structural disassembly of the DON. One of three independent experiments is shown.

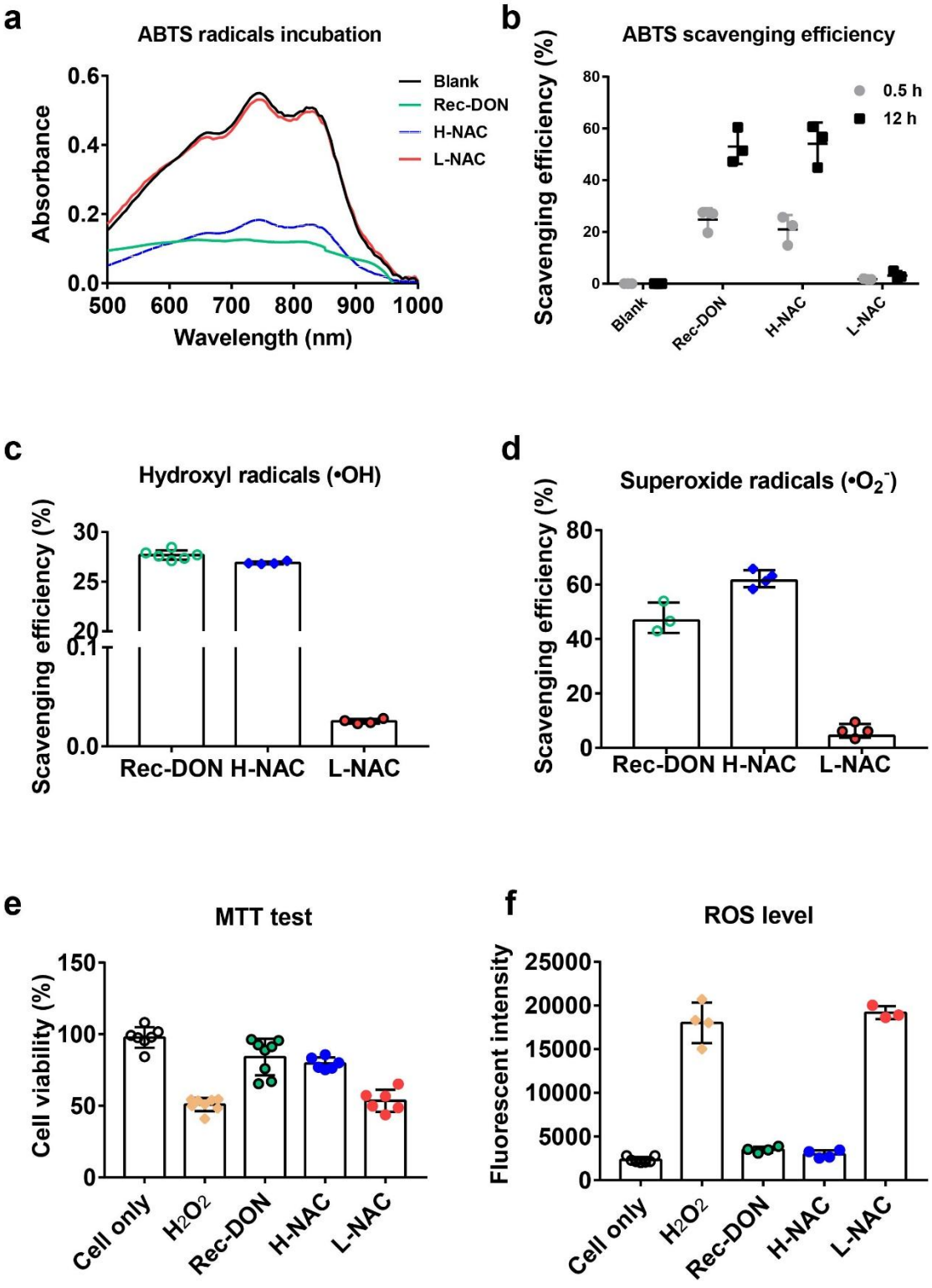

Figure S43. Comparison of ROS scavenging effect between Rec-DON and NAC. **(a)** UV-Vis spectra of ABTS radicals incubated with Rec-DON (5 nM), High dose NAC (H-NAC, 75 μM), or low dose NAC, (L-NAC, 5 nM). The characteristic absorbance of

ABTS radicals at 734 nm decreased after incubation with Rec-DON and H-NAC. One of three independent experiments is shown. **(b)** Analysis of ABTS radicals scavenging efficiency. Data represent mean ± standard deviation from three independent replicates. **(c)** Scavenging hydroxyl radicals (•OH) using Rec-DON (5 nM), H-NAC (75 µM), or L-NAC (5 nM). Data represent mean ± standard deviation from four independent replicates. **(d)** Scavenging superoxide radicals ($\bullet O_2^-$) using Rec-DON (5 nM), H-NAC (75 µM), or L-NAC (5 nM). Data represent mean ± standard deviation from three independent replicates. **(e)** Cell viability analysis when incubating HEK293 cells with H_2O_2 (250 µM) and Rec-DON, H-NAC, or L-NAC. Data represent mean ± standard deviation from six independent replicates. **(f)** ROS concentration when incubating HEK293 cells with H_2O_2 (250 µM) and Rec-DON, H-NAC, or L-NAC. Data represent mean ± standard deviation from three independent replicates.

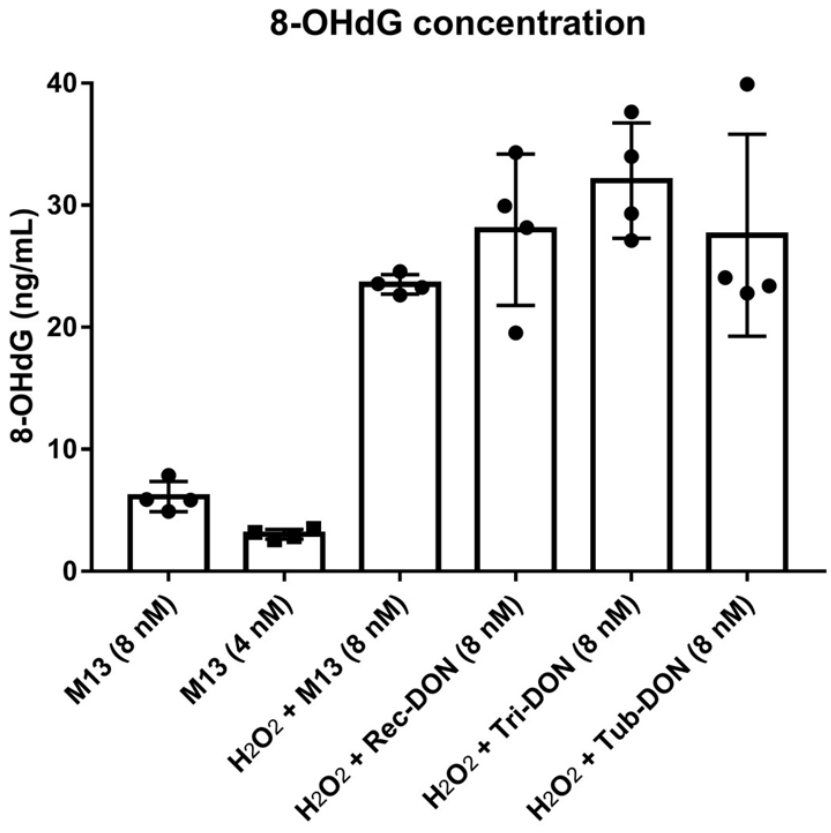

Figure S44. Concentration of 8-OHdG in three DONs incubated in H_2O_2 (250 mM) for 30 min. M13 was used as a control sample to establish the baseline level of 8-OHdG in solution. n=4. Data represent mean ± standard deviation.

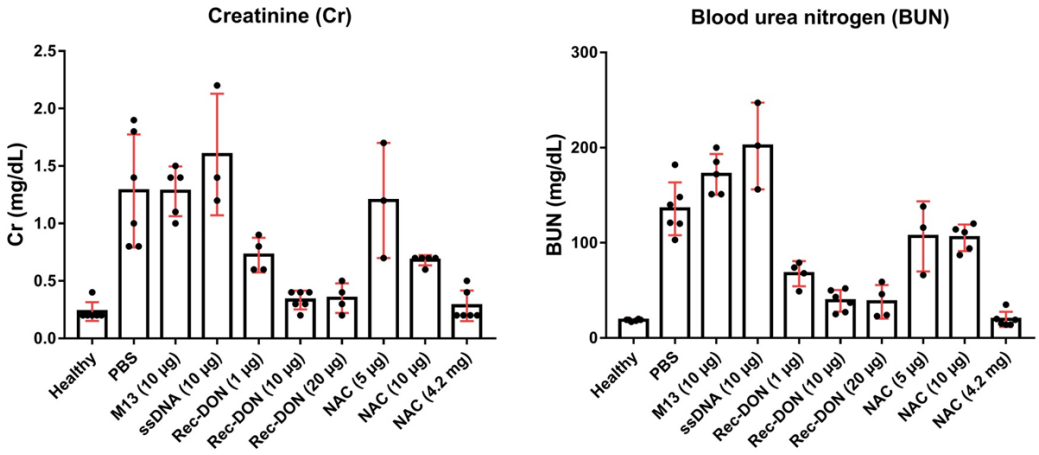

Figure S45. Analysis of serum creatinine (Cr, Left) and blood urea nitrogen (BUN, right) levels of AKI mice after treatment. Healthy mice were used as a control group. Lower levels of Cr and BUN indicate better kidney functions. n=3 for Group ssDNA (10 μg) and NAC (5 μg); n=4 for Group Rec-DON (1 μg) and Rec-DON (20 μg); n=5 for Group M13 (10 μg) and NAC (10 μg); n=6 for Group Healthy, PBS, Rec-DON (10 μg), and NAC (4.2 mg). Data represent mean ± standard deviation.

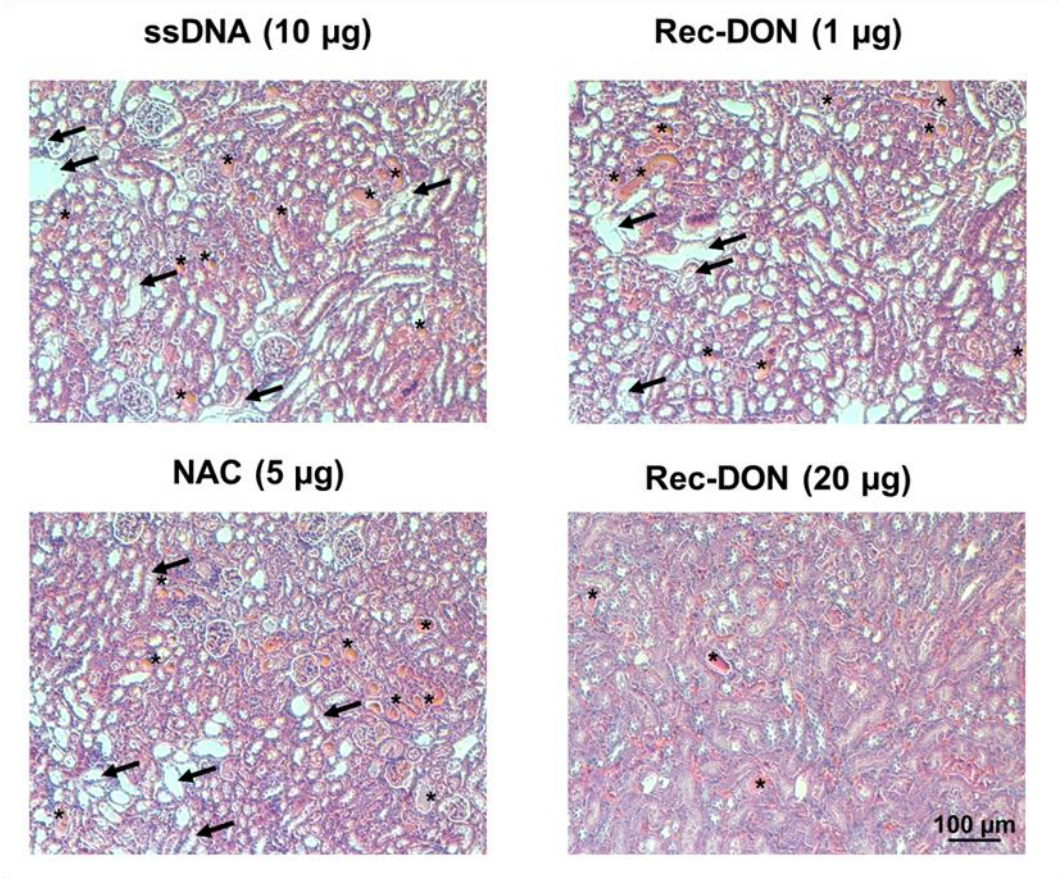

Figure S46. H&E staining of kidney tissues of AKI mice after various treatment regimens. Arrows denote damaged tubules, and asterisks denote the formation of casts, a structure formed via precipitation of denatured proteins in the tubules. Scale bar: 100 μm. One of three independent experiments was shown.

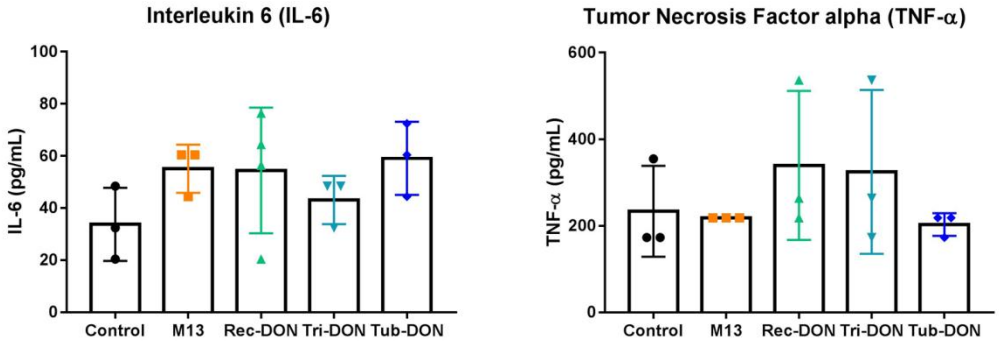

Figure S47. Serum levels of interleukin-6 (IL-6) and tumor necrosis factor alpha (TNF-α) at 24 h after *i.v.* injection of M13, Rec-DON, Tri-DON, or Tub-DON into healthy mice (10 μg DNA materials per mouse). n=3. Data represent mean ± standard deviation.

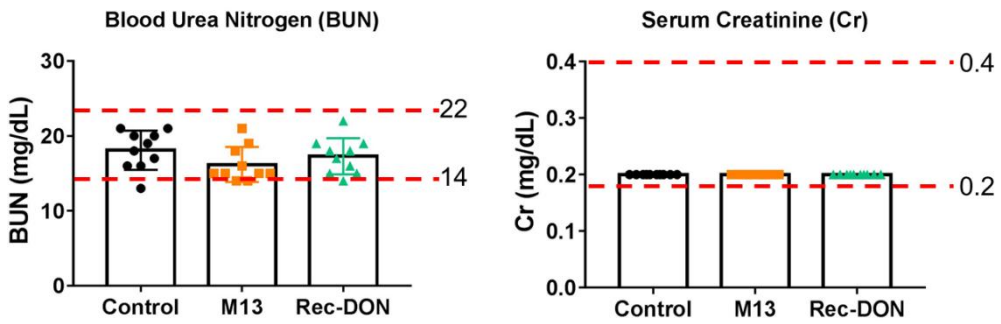

Figure S48. Serum levels of blood urea nitrogen (BUN) and creatinine (Cr) in healthy mice, and mice injected with M13 or Rec-DON (10 μg per mouse). Blood was collected at 24 h after injection. Dash lines denote the normal values and ranges of parameters for healthy mice. n=10. Data represent mean ± standard deviation.

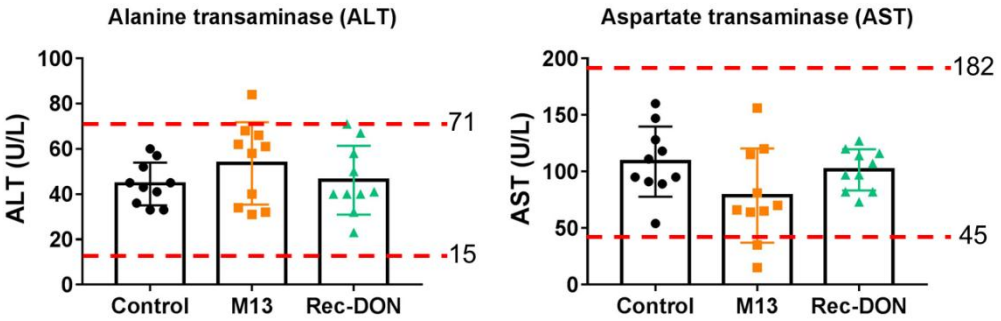

Figure S49. Serum levels of alanine transaminase (ALT) and aspartate transaminase (AST) in healthy mice, and mice injected with M13 or Rec-DON (10 μg per mouse). Blood was collected at 24 h after injection. Dash lines denote the normal values and ranges of parameters for healthy mice. n=10. Data represent mean ± standard deviation.

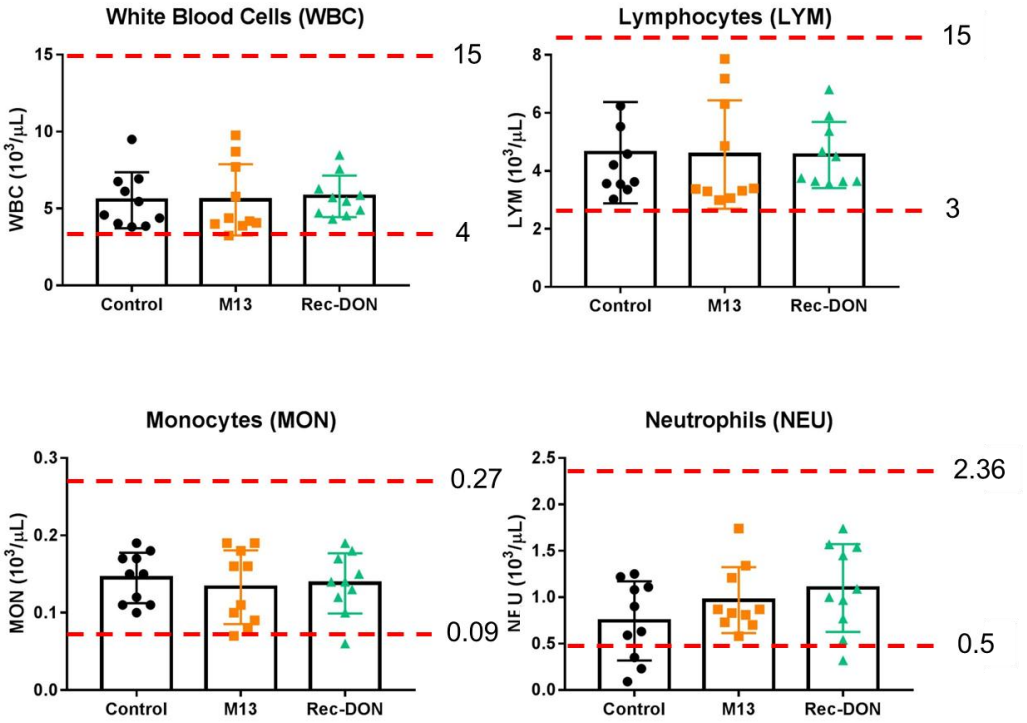

Figure S50. Numbers of white blood cells (WBC), lymphocytes (LYM), monocytes (MON), and neutrophils (NEU) in healthy mice, and mice injected with M13 or Rec-DON (10 μg per mouse). Blood was collected at 24 h after injection. Dash lines denote the normal values and ranges of parameters for healthy mice. n=10. Data represent mean ± standard deviation.

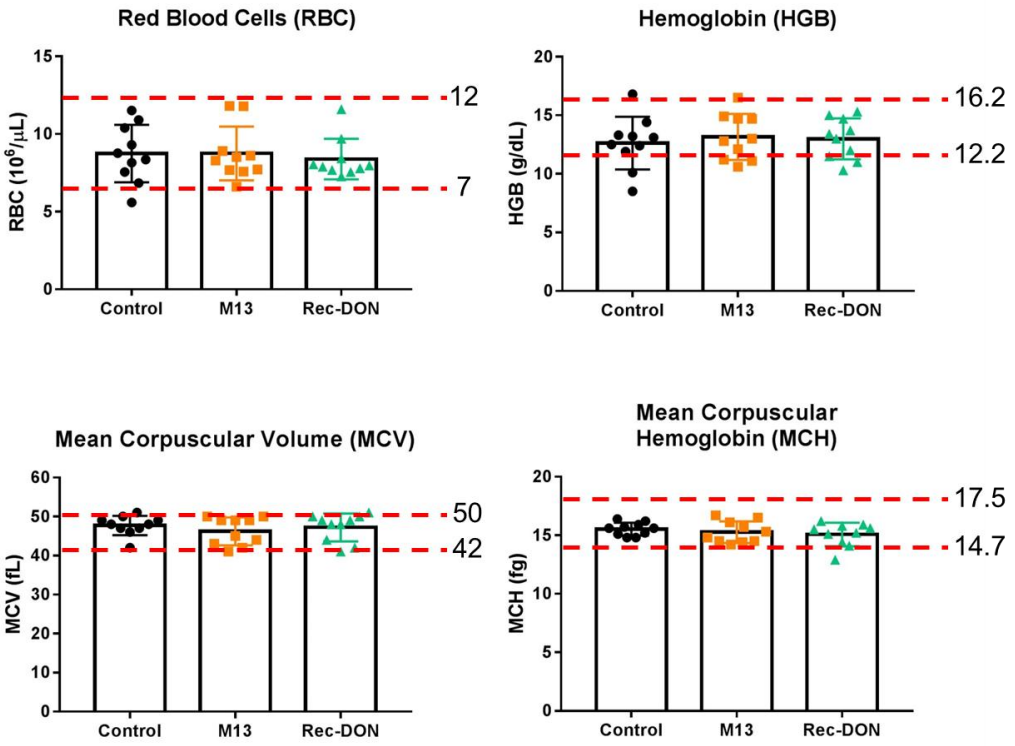

Figure S51. Numbers of red blood cells (RBC), hemoglobin (HGB), mean corpuscular volume (MCV), and mean corpuscular hemoglobin (MCH) in healthy mice, and mice injected with M13 or Rec-DON (10 μg per mouse). Blood was collected at 24 h after injection. Dash lines denote the normal values and ranges of parameters for healthy mice. n=10. Data represent mean ± standard deviation.

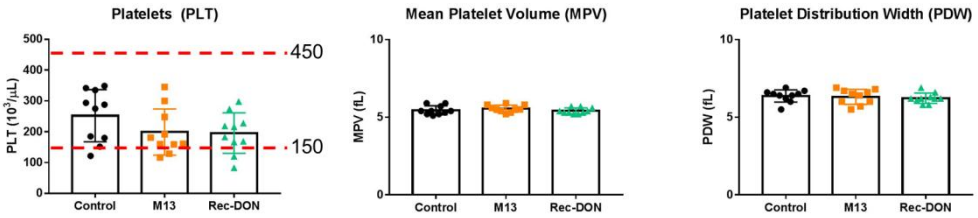

Figure S52. Numbers of platelets (PLT), mean platelet volume (MPV), and platelet distribution width (PDW) in healthy mice, and mice injected with M13 or Rec-DON (10 μg per mouse). Blood was collected at 24 h after injection. Dash lines denote the normal values and ranges of parameters for healthy mice. n=10. Data represent mean ± standard deviation.

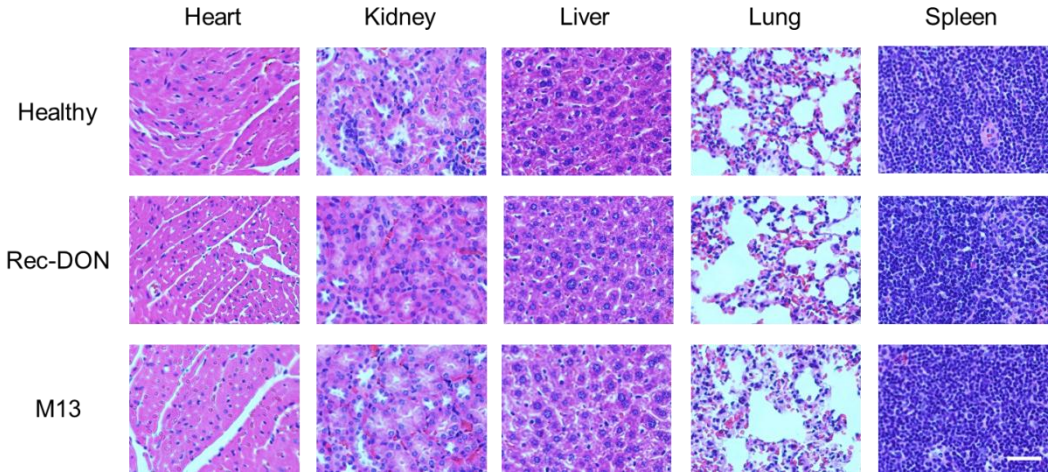

Figure S53. Representative H&E staining images (from one of three independent experiments) of primary organs of mice injected with Rec-DON or M13 (10 μg per mouse). Tissues from healthy mice were used as controls. No abnormality was observed. Scale bar: 100 μm.

Supplementary Table S1. Annealing program for self-assembly of DNA origami nanostructures. Each step represents 1 ºC of temperature change.

Annealing Protocol

Temperature	Time/Step
90 ºC	30 sec
86-71 ºC	1 min/step
70-60 ºC	10 min/step
59-30 ºC	15 min/step
29-26 ºC	10 min/step
25 ºC	25 min
4 ºC	Hold

Supplementary Table S2. Details of DNA materials used in this study.

DNA material	Number of Adenine (A)	Number of Guanine (G)	Number of Cytosine (C)	Number of Thymine (T)	Total bases	Molecular weight (g/mol)
M13	1768	1533	1538	2410	7249	2.2×10^6
Staple strands	2410	1538	1533	1768	7249	-
DONs	4178	3071	3071	4178	14498	4.4×10^6

Supplementary Table S3. Details of test materials used for AKI treatment.

Test materials	Molecular weight (g/mol)	Dose in μg	Dose in pmol	Volume (μL)	Conc. (nM)	Amount of reductants in nmol (DNA base or NAC)
PBS	---	---	---	200	---	0
M13	2.2×10^{6}	10	4.5	200	22.5	32.6
Rec-DON	4.4×10^{6}	10	2.3	200	11.5	33.3
H-NAC	163.19	4200	2.6×10^{6}	200	1.3×10^{7}	2.6×10^{3}
L-NAC	163.19	10	6.1×10^{4}	200	3.1×10^{5}	61

Supplementary Table S4. Oligonucleotides used for the assembly and radiolabeling of DNA tetrahedron nanoparticle (DTN) with overhangs.

Oligonucleotide	Sequence
Strand 1	5’-TTTTTTTTTTTTTTTTTTTTATTGCTGTATTGGCTCTGGTGATGCGTTAAAGGATCTCGTATAGCAGCTCAGTCCACTCGAAC-3’
Strand 2	5’-TTTTTTTTTTTTTTTTTTTTCATAGTCAATAACGCATCACCAGAGCCAAATGACGACATCTGTGCGATGAAACCTAGCAGACC-3’
Strand 3	5’-TTTTTTTTTTTTTTTTTTTTGAGATCCTATGACTATGGGTCTGCTAGGTACAGTCTGTCGCTTATGCACTAGAGCTGCTATAC-3’
Strand 4	5’-TTTTTTTTTTTTTTTTTTTTGTCGTCAAACAGCAATGTTCGAGTGGACAAGTGCATAAGCGACAGACTGATCATCGCACAGA-3’
ssDNA for radiolabeling	5‘-AAAAAAAAAAAAAAAAAAAA-NH2-3’

Supplementary Table S5. Statistical analysis of the MTT assay results from six independent replicates (**Figure 4e**). Statistical analysis was performed with one-way ANOVA with the Tukey's HSD post-hoc test. Cell viability was compared after HEK293 cells were incubated with H_2O_2 (250 μM) and treated with M13 ssDNA or different DONs (equal numbers of DNA bases).

Tukey's multiple comparisons test	Mean Diff.	Significant?	Summary	P Value
Cell only vs. H_2O_2	49.16	Yes	****	<0.0001
Cell only vs. M13	13.03	No	ns	0.2811
Cell only vs. Rec-DON	15.9	No	ns	0.0930
Cell only vs. Tri-DON	16.48	No	ns	0.0745
Cell only vs. Tub-DON	19.31	Yes	*	0.0425
H_2O_2 vs. M13	-36.13	Yes	****	<0.0001
H_2O_2 vs. Rec-DON	-33.26	Yes	****	<0.0001
H_2O_2 vs. Tri-DON	-32.68	Yes	****	<0.0001
H_2O_2 vs. Tub-DON	-29.85	Yes	***	0.0004
M13 vs. Rec-DON	2.877	No	ns	0.9967
M13 vs. Tri-DON	3.457	No	ns	0.9923
M13 vs. Tub-DON	6.287	No	ns	0.9252
Rec-DON vs. Tri-DON	0.5804	No	ns	>0.9999
Rec-DON vs. Tub-DON	3.41	No	ns	0.9941
Tri-DON vs. Tub-DON	2.83	No	ns	0.9975

Supplementary Table S6. Statistical analysis of the ROS assay results from four independent replicates (**Figure 4f)**. Statistical analysis was performed with one-way ANOVA with the Tukey's HSD post-hoc test. ROS concentration was compared after HEK293 cells were incubated with M13 ssDNA or different DONs (equal numbers of DNA bases) and then treated with H_2O_2 (250 µM).

Tukey's multiple comparisons test	Mean Diff.	Significant?	Summary	P Value
Control vs. H_2O_2	-15697	Yes	****	<0.0001
Control vs. M13	-9177	Yes	****	<0.0001
Control vs. Rec-DON	-1170	No	ns	0.6928
Control vs. Tri-DON	-1771	No	ns	0.2758
Control vs. Tub-DON	-1575	No	ns	0.3950
H_2O_2 vs. M13	6520	Yes	****	<0.0001
H_2O_2 vs. Rec-DON	14527	Yes	****	<0.0001
H_2O_2 vs. Tri-DON	13926	Yes	****	<0.0001
H_2O_2 vs. Tub-DON	14122	Yes	****	<0.0001
M13 vs. Rec-DON	8007	Yes	****	<0.0001
M13 vs. Tri-DON	7406	Yes	****	<0.0001
M13 vs. Tub-DON	7602	Yes	****	<0.0001
Rec-DON vs. Tri-DON	-601	No	ns	0.9841
Rec-DON vs. Tub-DON	-404.5	No	ns	0.9974
Tri-DON vs. Tub-DON	196.5	No	ns	>0.9999

Supplementary Table S7. Statistical analysis of the Clearance of ^{68}Ga-EDTA from kidneys to the bladder from three independent replicates (**Figure 5e**). Statistical analysis was performed with one-way ANOVA with the Tukey's HSD post-hoc test.

Tukey's multiple comparisons test	Mean Diff.	Significant?	Summary	P Value
Healthy vs. PBS	28.85	Yes	****	<0.0001
Healthy vs. M13	29.82	Yes	****	<0.0001
Healthy vs. Rec-DON	13.86	No	ns	0.0531
Healthy vs. H-NAC	12.29	No	ns	0.0726
Healthy vs. L-NAC	24.73	Yes	***	0.0002
PBS vs. M13	0.975	No	ns	0.9998
PBS vs. Rec-DON	-14.98	Yes	*	0.0204
PBS vs. H-NAC	-16.56	Yes	**	0.0049
PBS vs. L-NAC	-4.117	No	ns	0.8767
M13 vs. Rec-DON	-15.96	Yes	*	0.0127
M13 vs. H-NAC	-17.54	Yes	**	0.0030
M13 vs. L-NAC	-5.092	No	ns	0.7526
Rec-DON vs. H-NAC	-1.578	No	ns	0.9986
Rec-DON vs. L-NAC	10.87	No	ns	0.1357
H-NAC vs. L-NAC	12.44	Yes	*	0.0426

Supplementary Table S8. Statistical analysis of the slope of kidney ROI curves between 1 and 2 min after injection of ^{68}Ga-EDTA from three independent replicates (**Figure 5f)**. Statistical analysis was performed with one-way ANOVA with the Tukey's HSD post-hoc test.

Tukey's multiple comparisons test	Mean Diff.	Significant?	Summary	P Value
Healthy vs. PBS	1.144	Yes	***	0.0004
Healthy vs. M13	1.197	Yes	***	0.0002
Healthy vs. Rec-DON	0.5571	No	ns	0.0736
Healthy vs. H-NAC	0.4958	No	ns	0.1285
Healthy vs. L-NAC	0.9927	Yes	**	0.0013
PBS vs. M13	0.0524	No	ns	0.9996
PBS vs. Rec-DON	-0.5873	No	ns	0.0556
PBS vs. H-NAC	-0.6486	Yes	*	0.0312
PBS vs. L-NAC	-0.1516	No	ns	0.9513
M13 vs. Rec-DON	-0.6397	Yes	*	0.0339
M13 vs. H-NAC	-0.701	Yes	*	0.0190
M13 vs. L-NAC	-0.204	No	ns	0.8535
Rec-DON vs. H-NAC	-0.0613	No	ns	0.9992
Rec-DON vs. L-NAC	0.4357	No	ns	0.2154
H-NAC vs. L-NAC	0.497	No	ns	0.1271

Supplementary Table S9. Statistical analysis of the washout half-time ($T_{1/2}$) of kidney ROI curves (time interval between the peak tracer concentration and half of the peak value) from three independent replicates (**Figure 5g**). Statistical analysis was performed with one-way ANOVA with the Tukey's HSD post-hoc test.

Tukey's multiple comparisons test	Mean Diff.	Significant?	Summary	P Value
Healthy vs. PBS	-161.1	Yes	**	0.0031
Healthy vs. M13	-133.1	Yes	*	0.0133
Healthy vs. Rec-DON	0.75	No	ns	>0.9999
Healthy vs. H-NAC	-6.657	No	ns	>0.9999
Healthy vs. L-NAC	-125.2	Yes	*	0.0201
PBS vs. M13	28	No	ns	0.9463
PBS vs. Rec-DON	161.8	Yes	**	0.0030
PBS vs. H-NAC	154.4	Yes	**	0.0044
PBS vs. L-NAC	35.87	No	ns	0.8652
M13 vs. Rec-DON	133.8	Yes	*	0.0128
M13 vs. H-NAC	126.4	Yes	*	0.0189
M13 vs. L-NAC	7.873	No	ns	0.9998
Rec-DON vs. H-NAC	-7.407	No	ns	0.9999
Rec-DON vs. L-NAC	-125.9	Yes	*	0.0193
H-NAC vs. L-NAC	-118.5	Yes	*	0.0285

Supplementary Table S10. Statistical analysis of the body weight changes from four independent replicates (**Figure 6a**). Statistical analysis was performed with one-way ANOVA with the Tukey's HSD post-hoc test.

Tukey's multiple comparisons test	Mean Diff.	Significant?	Summary	P Value
Healthy vs. PBS	10.63	Yes	**	0.0021
Healthy vs. M13	7.76	Yes	*	0.0123
Healthy vs. Rec-DON	2.07	No	ns	0.9397
Healthy vs. H-NAC	0.6571	No	ns	0.9998
Healthy vs. L-NAC	8.994	Yes	**	0.0042
PBS vs. M13	-2.874	No	ns	0.7937
PBS vs. Rec-DON	-8.563	Yes	*	0.0169
PBS vs. H-NAC	-9.976	Yes	**	0.0069
PBS vs. L-NAC	-1.639	No	ns	0.9792
M13 vs. Rec-DON	-5.69	No	ns	0.1087
M13 vs. H-NAC	-7.103	Yes	*	0.0422
M13 vs. L-NAC	1.235	No	ns	0.9886
Rec-DON vs. H-NAC	-1.413	No	ns	0.9910
Rec-DON vs. L-NAC	6.925	Yes	*	0.0396
H-NAC vs. L-NAC	8.337	Yes	*	0.0154

Supplementary Table S11. Statistical analysis of the serum creatinine levels from five independent replicates (**Figure 6b**). Statistical analysis was performed with one-way ANOVA with the Tukey's HSD post-hoc test.

Tukey's multiple comparisons test	Mean Diff.	Significant?	Summary	P Value
Healthy vs. PBS	-1.05	Yes	****	<0.0001
Healthy vs. M13	-1.047	Yes	****	<0.0001
Healthy vs. Rec-DON	-0.1	No	ns	0.9759
Healthy vs. H-NAC	-0.05	No	ns	0.9990
Healthy vs. L-NAC	-0.4467	Yes	*	0.0427
PBS vs. M13	0.003333	No	ns	>0.9999
PBS vs. Rec-DON	0.95	Yes	****	<0.0001
PBS vs. H-NAC	1	Yes	****	<0.0001
PBS vs. L-NAC	0.6033	Yes	**	0.0029
M13 vs. Rec-DON	0.9467	Yes	****	<0.0001
M13 vs. H-NAC	0.9967	Yes	****	<0.0001
M13 vs. L-NAC	0.6	Yes	**	0.0048
Rec-DON vs. H-NAC	0.05	No	ns	0.9990
Rec-DON vs. L-NAC	-0.3467	No	ns	0.1817
H-NAC vs. L-NAC	-0.3967	No	ns	0.0915

Supplementary Table S12. Statistical analysis of the blood urea nitrogen levels from five independent replicates (**Figure 6c**). Statistical analysis was performed with one-way ANOVA with the Tukey's HSD post-hoc test.

Tukey's multiple comparisons test	Mean Diff.	Significant?	Summary	P Value
Healthy vs. PBS	-117	Yes	****	<0.0001
Healthy vs. M13	-153.1	Yes	****	<0.0001
Healthy vs. Rec-DON	-20.33	No	ns	0.2875
Healthy vs. H-NAC	-0.8333	No	ns	>0.9999
Healthy vs. L-NAC	-86.53	Yes	****	<0.0001
PBS vs. M13	-36.13	Yes	*	0.0120
PBS vs. Rec-DON	96.67	Yes	****	<0.0001
PBS vs. H-NAC	116.2	Yes	****	<0.0001
PBS vs. L-NAC	30.47	Yes	*	0.0468
M13 vs. Rec-DON	132.8	Yes	****	<0.0001
M13 vs. H-NAC	152.3	Yes	****	<0.0001
M13 vs. L-NAC	66.6	Yes	****	<0.0001
Rec-DON vs. H-NAC	19.5	No	ns	0.3303
Rec-DON vs. L-NAC	-66.2	Yes	****	<0.0001
H-NAC vs. L-NAC	-85.7	Yes	****	<0.0001

Supplementary Table S13. Statistical analysis of the superoxide dismutase (SOD) levels from three independent replicates (**Figure 6d**). Statistical analysis was performed with one-way ANOVA with the Tukey's HSD post-hoc test.

Tukey's multiple comparisons test	Mean Diff.	Significant?	Summary	P Value
Healthy vs. PBS	9.31	Yes	****	<0.0001
Healthy vs. M13	8.733	Yes	****	<0.0001
Healthy vs. Rec-DON	1.782	No	ns	0.3020
Healthy vs. H-NAC	0.4193	No	ns	0.9943
Healthy vs. L-NAC	8.541	Yes	****	<0.0001
PBS vs. M13	-0.5765	No	ns	0.9765
PBS vs. Rec-DON	-7.528	Yes	****	<0.0001
PBS vs. H-NAC	-8.891	Yes	****	<0.0001
PBS vs. L-NAC	-0.7687	No	ns	0.9245
M13 vs. Rec-DON	-6.951	Yes	****	<0.0001
M13 vs. H-NAC	-8.314	Yes	****	<0.0001
M13 vs. L-NAC	-0.1922	No	ns	0.9999
Rec-DON vs. H-NAC	-1.363	No	ns	0.5632
Rec-DON vs. L-NAC	6.759	Yes	****	<0.0001
H-NAC vs. L-NAC	8.122	Yes	****	<0.0001

Reference

1. Ke YG, Lindsay S, Chang Y, Liu Y, Yan H. Self-assembled water-soluble nucleic acid probe tiles for label-free RNA hybridization assays. *Science* 2008, **319**(5860)**:** 180-183.

2. Lin M, Wang J, Zhou G, Wang J, Wu N, Lu J*, et al.* Programmable engineering of a biosensing interface with tetrahedral DNA nanostructures for ultrasensitive DNA detection. *Angew. Chem. Int. Ed. Engl.* 2015, **54**(7)**:** 2151-2155.

3. Jiang D, Sun Y, Li J, Li Q, Lv M, Zhu B*, et al.* Multiple-armed tetrahedral dna nanostructures for tumor-targeting, dual-modality in vivo imaging. *ACS Appl. Mater. Interfaces* 2016, **8**(7)**:** 4378-4384.

4. Singh AP, Muthuraman A, Jaggi AS, Singh N, Grover K, Dhawan R. Animal models of acute renal failure. *Pharmacol. Rep.* 2012, **64**(1)**:** 31-44.

5. Huang H, Hernandez R, Geng J, Sun H, Song W, Chen F*, et al.* A porphyrin-PEG polymer with rapid renal clearance. *Biomaterials* 2016, **76:** 25-32.

6. Hofman M, Binns D, Johnston V, Siva S, Thompson M, Eu P*, et al.* ^{68}Ga-EDTA PET/CT imaging and plasma clearance for glomerular filtration rate quantification: comparison to conventional ^{51}Cr-EDTA. *J. Nucl. Med.* 2015, **56**(3)**:** 405-409.